J. Fluid Mech. (1993), *vol.* 250, *pp.* 307–337

Dynamic simulations of flows of bubbly liquids at large Reynolds numbers

By A. S. SANGANI AND A. K. DIDWANIA†
Department of Chemical Engineering and Materials Science, Syracuse University, Syracuse, NY 13244, USA

(Received 2 January 1992 and in revised form 18 May 1992)

Results of dynamic simulations of bubbles rising through a liquid are presented. The Reynolds number of the flow based on the radius and the terminal speed of bubbles is large compared to unity, and the Weber number, which is the ratio of inertial to surface tension forces, is small. It is assumed that the bubbles do not coalesce when they approach each other but rather bounce instantaneously, conserving the momentum and the kinetic energy of the system. The flow of the liquid is assumed to be irrotational and is determined by solving the many-bubble interaction problem exactly. The viscous force on the bubbles is estimated from the rate of viscous energy dissipation. It is shown that the random state of bubbly liquids under these conditions is unstable and that the bubbles form aggregates in planes transverse to gravity. These aggregates form even when the size distribution of the bubbles is non-uniform. While the instability results primarily from the nature of inertial interaction among pairs of bubbles, which causes them to be attracted toward each other when they are aligned in the plane perpendicular to gravity, it is shown that the presence of viscous forces facilitates the process.

1. Introduction

Flows of gas–liquid dispersions occur in a variety of industrial and natural processes, and therefore the problem of describing such flows quantitatively has been the subject of numerous investigations. In particular, one of the central problems is to obtain a set of averaged equations that govern the flow of liquids in which the bubbles are uniformly dispersed and to predict the conditions under which such a state becomes unstable. For quantitative analyses, it is necessary not only to derive the correct form of these equations but also to obtain reliable estimates of the various averaged quantities, such as the added mass and viscous drag coefficients, that appear in the averaged equations. These quantities can be determined with the help of dynamic simulations. The simulations are needed because the macroscopic properties depend on the details of the microstructure of the dispersion and these details in turn depend on the nature of the macroscopic flow. In addition to providing estimates of various properties, the simulations can help to understand the relationship between the microstructure and the properties of bubbly liquids.

We consider here a relatively simple macroscopic flow generated by the buoyancy forces acting on the bubbles in an infinitely extended homogeneous dispersion. The Reynolds number Re of the flow based on the radius a and terminal rise velocity V^*

† Present address: Department of Applied Mechanics and Engineering Sciences, University of California, San Diego, CA 92093-0310, USA.

of the bubbles is assumed to be large. The effect of finite viscosity is assumed to be confined to a small region near the surface of the bubbles. It has been observed experimentally that, when the concentration of the surface-active impurities in the dispersion is small, there is no separation of the viscous boundary layer from the surface of a bubble, and the theoretical analysis of Moore (1963) has shown that the size of the stagnation region behind a bubble under such conditions is small compared to the radius of the bubble. More specifically, Moore analysed the problem of steady uniform flow past a spherical bubble and showed that the velocity field to leading order can be considered to be irrotational or potential everywhere in the liquid, and that the correction to this is $O(Re^{-\frac{1}{2}})$ in the thin boundary layer of thickness $O(Re^{-\frac{1}{2}})$ near the surface of the bubble. He also showed that the wake behind the bubble is small, of diameter $O(Re^{-\frac{1}{4}})$, in contrast to the flow past a solid sphere for which there is a boundary-layer separation causing a finite region of recirculation. While it is not clear if his arguments are entirely valid even for the case of flows of bubbly liquids at finite volume fractions of the gas bubbles, where the flow around individual bubbles is never steady due to complex interactions among the bubbles, we shall assume that the flow can be approximated to leading order, $O(Re^0)$, as irrotational everywhere in the dispersion.

To keep the analysis relatively simple, we further assume that the bubbles do not coalesce and that they remain spherical. The latter requires that the Weber number, which is the ratio of the surface tension forces to the inertial forces, be small compared to unity. For the air–water system, the conditions of large Reynolds number and small Weber number are satisfied by bubbles approximately 1 mm in diameter. Careful experimental observations of the dynamics of a pair of bubbles of this size rising under the influence of gravity have been reported by Kok (1989). He observed that when the two air bubbles approach each other, due to hydrodynamic interactions between them in pure water, they generally coalesce. If, however, a small amount of surface-active impurities is added to the same system, then the two bubbles do not coalesce but, rather, bounce instantaneously. He also calculated analytically the trajectories of the bubbles using a potential flow approximation together with the viscous forces estimated by the viscous energy dissipation method and showed that the trajectories thus evaluated matched very closely with those observed experimentally. Finally, he also carried out experiments with moderate to high concentrations of the surface-active impurities and found that the potential flow approximation was not valid for such a situation. The surfaces of the bubbles become considerably immobile at high concentrations of the surface-active impurities, resulting in a finite-size recirculation region behind the bubbles and much more complicated hydrodynamics. Thus, the calculations we carry out here are likely to be applicable to gas–liquid dispersions in the presence of a small amount of surface-active impurities.

Finally, we shall assume that the radius of the bubbles remains unchanged throughout the flow. This is a good approximation since $\rho V^{*2}/P_a$ is usually small compared to unity. Here ρ is the density of the liquid and P_a is the atmospheric pressure.

We describe here a method for carrying out dynamic simulations of the flow under the aforementioned conditions. To simulate the condition of macroscopic homogeneity, we place N bubbles initially randomly within a unit cell and assume that the entire space is filled with the copies of this cell. We determine the potential flow around many bubbles exactly by using a method of multipole expansions. The drag force is determined using two different methods, both yielding the same results. One is based on computing the gradient of the rate of total viscous energy dissipation with the

velocity of the individual bubble – the method employed previously by Kok (1989) in comparing his experimentally observed trajectories with the calculated ones as described earlier, and the other is based on a recent analysis of small-amplitude oscillatory flows past bubbles by Sangani (1991). The bounce of the colliding bubbles is determined from the assumption that the collision time is short compared to the timescale for the inertial motion and that the momentum and the kinetic energy of the system is conserved during the collision. We show that the normal component of the relative motion of the colliding pair of bubbles reverses its direction upon collision just as in the case of collision between two elastic spheres in vacuum, but unlike the latter case, all the other bubbles in the dispersion also undergo a change in their velocities whenever any two bubbles collide. This is a consequence of the fact that the bubbles are essentially massless and that the momentum and the kinetic energy of the system is entirely contained by the liquid.

We find that the state of uniform bubbly liquids is unstable under the aforementioned conditions and that the bubbles form large aggregates by arranging themselves in planes perpendicular to gravity. These aggregates form even when the initial velocity and size distributions of bubbles are non-uniform, provided that the degree of the latter is not too high. Finally, we also show that such large aggregates form even when a swarm of gas bubbles rises through a liquid at rest at infinity.

The above results correspond to the case in which we include the buoyancy and viscous forces in the simulations. We have also carried out dynamic simulations for the case in which these forces are absent, and found that the bubbles do not form the planar aggregates if the initial velocity distribution is sufficiently non-uniform. Thus, the presence of viscous forces is important for the formation of large aggregates. In purely inertial interactions, the overall momentum and kinetic energy is conserved and the subsequent development of the microstructure must satisfy these constraints, whereas the presence of viscous forces allows the momentum and kinetic energy of the system to vary in a manner that facilitates the formation of planar aggregates.

We should add here that the previous studies by Biesheuvel & van Wijngaarden (1982) and Kok (1989), which examined the interaction of a pair of bubbles, have shown that the pair has a tendency to align itself in a plane perpendicular to gravity as a result of the inertial interactions. This is a simple consequence of the inviscid pressure distribution for the pair of bubbles. The pressure in the gap between the bubbles is small compared to the ambient pressure when the pair is aligned perpendicular to the flow, and this results in attractive forces between the bubbles. The opposite is true for a pair aligned parallel to the flow. That the pair of bubbles indeed aligns perpendicular to the flow has also been observed experimentally by Kok (1989).

Based on the above discussion then, one would expect the planar aggregates to form from an initial random distribution within a timescale that is related to the amount of polydispersivity, initial velocity distribution, the volume fraction of bubbles β, and the Reynolds number. From our simulations for $\beta = 0.1$ and $Re = 500$, we estimate this time for a monodispersed air bubbles to be only 0.1 s. To our knowledge, however, such large planar aggregates have not been the subject of any experimental investigation and the reason for this apparent discrepancy is not clear to us. However, it should be mentioned here that the majority of the large Reynolds number flow visualizations and measurements have been carried out under conditions in which either the effect of the macroscale flow instabilities such as turbulence or the macroscopic flow generated due to uneven distribution of the bubbles in the vessel cannot be ruled out. Finally, the bubble size distribution is difficult to control in experiments, and the size of bubbles generated in typical experiments is often such that they cannot be assumed to be

spherical in shape. Nonetheless, what the present study shows is that the simple set of approximations made here is not adequate to explain the experimental observations on the rise of bubbles through a liquid, and that we shall need to invoke further hypotheses or mechanisms which may be responsible for stabilizing the uniform flow of bubbly liquids. It is quite likely that the average properties of the bubbly liquids will then explicitly depend on the mechanism we choose for stabilizing. Finally, it should also be noted that there are other kinds of flows of bubbly liquids, e.g. shear flows, where behaviour may be quite different, and for which the simple approximations used in the present analysis may be adequate.

The organization of the paper is as follows. In §2, we describe in detail the method used for the simulation. The many-bubble interaction problem has been solved exactly by the method of multipole expansions discussed more fully in Sangani & Yao (1988) and Sangani, Zhang & Prosperetti (1991). The calculations for the trajectories of the bubbles, their collisions, and an estimation of the viscous drag on them are new and so described in detail. The results are presented in §3, and concluding remarks in §4.

2. The simulation method

As mentioned in the Introduction, our goal is to simulate the motion in an infinitely extended bubbly liquid which is homogeneous on a macroscale. To achieve this, we assume that the entire space is filled with identical cubic cells with each cell containing N randomly placed bubbles with a specified initial velocity distribution. The flow past bubbles at large Reynolds numbers can be regarded as irrotational, and hence it can be derived from a velocity potential which satisfies the Laplace equation. We therefore describe first how we determine the potential flow around many bubbles.

2.1. *A solution for the potential flow around many bubbles*

The potential flow around bubbles can be determined by solving the Laplace equation

$$\nabla^2\phi = 0, \tag{1}$$

where the potential ϕ is related to the velocity field by $\boldsymbol{u} = \nabla\phi$. When the Weber number is small, the bubbles may be assumed to remain approximately spherical, and the boundary condition for determining the above potential is the usual kinematic condition

$$\boldsymbol{n}\cdot\nabla\phi = \boldsymbol{n}\cdot\boldsymbol{v}^\alpha \tag{2}$$

on the surface S^α of the bubble α. Here, $\boldsymbol{n}$ is the unit outward normal from S^α. As we shall see later, the velocity $\boldsymbol{v}^\alpha$ of the bubble may not be known *a priori*. Instead, the impulse as defined by

$$\boldsymbol{I}^\alpha = -\rho\int_{S^\alpha}\phi\boldsymbol{n}\,\mathrm{d}A \tag{3}$$

may be specified. Note that in this case $\boldsymbol{v}^\alpha$ is an unknown to be determined as a part of the solution.

A solution of (1) satisfying the periodicity requirement can be expressed in terms of multipole expansions as described in Sangani & Yao (1988) and Sangani *et al.* (1991). Thus, we write

$$\phi(\boldsymbol{x},t) = \boldsymbol{G}\cdot\boldsymbol{x} + \sum_{\alpha=1}^{N}\sum_{n=1}^{\infty}\sum_{m=0}^{n}(A^\alpha_{nm}\Delta_m + \tilde{A}^\alpha_{nm}\tilde{\Delta}_m)\frac{\partial^{n-m}}{\partial x_1^{n-m}}S_1(\boldsymbol{x}-\boldsymbol{x}^\alpha), \tag{4}$$

where
$$\Delta_m = \left(\frac{\partial}{\partial\xi}\right)^m + \left(\frac{\partial}{\partial\eta}\right)^m, \quad \tilde{\Delta}_m = \mathrm{i}\left[\left(\frac{\partial}{\partial\xi}\right)^m - \left(\frac{\partial}{\partial\eta}\right)^m\right], \tag{5}$$

with $\xi = x_2 + \mathrm{i}x_3$ and $\eta = x_2 - \mathrm{i}x_3$. S_1 is a periodic Green's function for the Laplace equation that satisfies

$$\nabla^2 S_1(\boldsymbol{x}) = 4\pi\left[\tau^{-1} - \sum_{\boldsymbol{x}_L} \delta(\boldsymbol{x} - \boldsymbol{x}_L)\right], \tag{6}$$

with τ being the volume of the unit cell and $\boldsymbol{x}_L$ the lattice vectors for the periodic array. The function S_1 was introduced by Hasimoto (1959) and an expression for evaluating this function and its derivatives by Ewald's technique is given in Sangani *et al.* (1991). The function S_1 itself does not satisfy the Laplace equation but its derivatives do (except at the lattice points), and therefore the term with $n = 0$ is excluded from the above expression for ϕ. Actually, the coefficients with $n = 0$ correspond to monopoles which are needed only when there are fluctuations in the volume of the bubbles. Since the dynamic pressure which scales as ρV^2 is much smaller than the atmospheric pressure, the magnitude of volume fluctuations is negligible. The coefficients A^α_{nm} and $\tilde{A}^\alpha_{nm}$ may be referred to as the strengths of 2^n-multipoles located at the centre of the bubble α, and $\boldsymbol{G}$ is related to the mean velocity of the mixture. Both $\boldsymbol{G}$ and the strengths of multipoles are, in general, functions of time and are to be evaluated from the boundary conditions on the bubbles. The mean mixture velocity is evaluated from

$$\tau \boldsymbol{U} = \int_{\tau_f} \nabla\phi \, \mathrm{d}V + \sum_{\alpha=1}^{N} \sigma^\alpha \boldsymbol{v}^\alpha, \tag{7}$$

where τ_f is the volume occupied by the fluid within the basic unit cell and $\sigma^\alpha = \frac{4}{3}\pi a^{\alpha 3}$ is the volume of the bubble α, a^α being its radius. The volume integral on the right-hand side of (7) can be readily evaluated using the divergence theorem to yield

$$\boldsymbol{U} - \boldsymbol{G} = \frac{1}{\tau}\sum_{\alpha=1}^{N} (\sigma^\alpha \boldsymbol{v}^\alpha + \rho^{-1}\boldsymbol{I}^\alpha), \tag{8}$$

where $\boldsymbol{I}^\alpha$ is the impulse associated with the bubble α as defined by (3). The dynamic simulations can be carried out under the conditions of either constant $\boldsymbol{U}$ or constant $\boldsymbol{G}$. The latter can be shown to correspond to the case in which the pressure drop across the unit cell and the average velocity of the liquid remain constant throughout the simulation. Thus, we shall assume that one of the two quantities, i.e. $\boldsymbol{G}$ or $\boldsymbol{U}$, is specified, and the other is then determined from (8). It should also be noted that the constant quantity ($\boldsymbol{U}$ or $\boldsymbol{G}$) may be chosen to be zero without loss of generality.

To determine the strengths of multipoles, we follow the method outlined in Sangani & Yao (1988) and expand ϕ in a series of surface harmonics around the centre of the bubble α as

$$\phi = \sum_{n=0}^{\infty}\sum_{m=0}^{n} f^\alpha_{nm}(s)\, Y_{nm} + \tilde{f}^\alpha_{nm}(s)\, \tilde{Y}_{nm}, \tag{9}$$

where $Y_{nm} = P_n^m(\cos\theta)\cos m\varphi$, $\tilde{Y}_{nm} = P_n^m(\cos\theta)\sin m\varphi$, and (s, θ, φ) are the spherical polar coordinates of a point $\boldsymbol{x}$ with respect to the centre of bubble α, i.e.

$$x_1 - x_1^\alpha = s\cos\theta, \quad x_2 - x_2^\alpha = s\sin\theta\cos\varphi, \quad x_3 - x_3^\alpha = s\sin\theta\sin\varphi. \tag{10}$$

The functions f^α_{nm} can be expressed as

$$f^\alpha_{nm}(s) = C^\alpha_{nm}\, s^n + D^\alpha_{nm}\, s^{-n-1}. \tag{11}$$

The coefficients C^{α}_{nm} and D^{α}_{nm} can be evaluated from the observation that they must be related, respectively, to the regular and singular parts of ϕ at $s = 0$. Thus, as shown in Sangani & Yao (1988), we have

$$D^{\alpha}_{nm} = (-1)^{n-m}(n-m)!2^{1-m}A^{\alpha}_{nm}, \tag{12}$$

$$C^{\alpha}_{nm} = \frac{1}{(n+m)!}\frac{(-2)^m}{1+\delta_{m0}}\left[\left(\frac{\partial}{\partial x_1}\right)^{n-m}\Delta_m\phi^{(r)}\right]_{x=x^{\alpha}}, \tag{13}$$

where $\phi^{(r)}$ is the regular part of ϕ in the neighbourhood of x^{α}. Since the singular part of $S_1(x-x^{\alpha})$ is $1/s$ (Hasimoto 1959), $\phi^{(r)}$ is given by

$$\phi^{(r)}(x) = \phi(x) - \sum_{k=1}^{\infty}\sum_{j=0}^{k}(A^{\alpha}_{kj}\Delta_j + \tilde{A}^{\alpha}_{kj}\tilde{\Delta}_j)\left(\frac{\partial}{\partial x_1}\right)^{k-j}\frac{1}{|x-x^{\alpha}|}. \tag{14}$$

The expression for $\tilde{f}^{\alpha}_{nm}$ similarly contains $\tilde{C}^{\alpha}_{nm}$ and $\tilde{D}^{\alpha}_{nm}$, which, in turn, can be evaluated from expressions similar to (12) and (13) with A^{α}_{nm} and Δ_m in those relations replaced by the corresponding quantities with tildes.

The expansion of ϕ near the surface of the bubble α as given by (9) is particularly useful for satisfying the boundary condition on the surface of that bubble. Thus, on noting that $\boldsymbol{n}\cdot\boldsymbol{u}$ is related to the radial derivative of f^{α}_{nm}, and that $n_1 = Y_{10}$, $n_2 = -Y_{11}$, and $n_3 = -\tilde{Y}_{11}$, the use of orthogonality of the surface harmonics yields

$$f^{\alpha\prime}_{nm}(a^{\alpha}) = \tilde{f}^{\alpha\prime}_{nm}(a^{\alpha}) = 0, \quad n \geqslant 2, \tag{15}$$

$$f^{\alpha\prime}_{10}(a^{\alpha}) = v^{\alpha}_1, \quad f^{\alpha\alpha}_{11}(a^{\alpha}) = -v^{\alpha}_2, \quad \tilde{f}^{\alpha\prime}_{11}(a^{\alpha}) = -v^{\alpha}_3, \tag{16}$$

where the prime indicates the derivative of the function with respect to its argument. The above relations can be used to provide an equation for relating C^{α}_{nm} to D^{α}_{nm}. For example, combining (11) and (15), we obtain

$$C^{\alpha}_{nm} - \frac{n+1}{n}a^{\alpha^{-2n-1}}D^{\alpha}_{nm} = 0, \quad n \geqslant 2 \tag{17}$$

plus a similar relation between the corresponding quantities with tilde. It is convenient to group the coefficients with $n = 1$ into a vector. Thus, let

$$\boldsymbol{C}^{\alpha}_1 = C^{\alpha}_{10}\boldsymbol{e}_1 - C^{\alpha}_{11}\boldsymbol{e}_2 - \tilde{C}^{\alpha}_{11}\boldsymbol{e}_3 \tag{18}$$

and

$$\boldsymbol{D}^{\alpha}_1 = D^{\alpha}_{10}\boldsymbol{e}_1 - D^{\alpha}_{11}\boldsymbol{e}_2 - \tilde{D}^{\alpha}_{11}\boldsymbol{e}_3 = -2A^{\alpha}_{10}\boldsymbol{e}_1 - A^{\alpha}_{11}\boldsymbol{e}_2 - \tilde{A}^{\alpha}_{11}\boldsymbol{e}_3, \tag{19}$$

$\boldsymbol{e}_1$, $\boldsymbol{e}_2$, and $\boldsymbol{e}_3$ being the unit vectors along the three coordinate axes. The relations for $n = 1$ (cf. (16)) can be expressed as

$$\boldsymbol{C}^{\alpha}_1 - 2\boldsymbol{D}^{\alpha}_1 a^{\alpha^{-3}} = \boldsymbol{v}^{\alpha}. \tag{20}$$

If the impulse associated with the bubble is specified, then, instead of the above relation, we must use

$$\boldsymbol{I}^{\alpha} = -\rho\sigma^{\alpha}(\boldsymbol{C}^{\alpha}_1 + \boldsymbol{D}^{\alpha}_1 a^{\alpha^{-3}}), \tag{21}$$

obtained by making use of (3) and (11) and noting that the components of the unit normal vector $\boldsymbol{n}$ on the surface of a sphere are related to the surface harmonics of first order.

2.2. *Viscous forces*

The viscous forces, although small in magnitude for large Reynolds number flows, play an important role in determining the magnitude of the average relative velocity and the microstructure of the dispersion. In the large Reynolds number flows past free surfaces, at which the tangential stress vanishes but not the relative tangential velocity, vorticity generation is weak and the effect of viscosity is confined to a thin layer adjacent to the surface (see, for example, Batchelor 1967). The boundary-layer analysis of uniform flow past a spherical bubble by Moore (1963) has shown that, in these conditions, the correction to the velocity as derived from the potential flow approximation is uniformly small everywhere in the limit $Re \to \infty$. This analysis, however, cannot be applied to evaluate the viscous force on each bubble to leading order, $O(Re^{-1})$, as the boundary-layer approximation of Moore (1963) breaks down near the rear stagnation point so that the correction to the viscous drag from the viscous correction to the pressure in the wake behind the bubble is difficult to evaluate. Tam (1981) has addressed this problem, but his results are inconclusive.

For the case of steady translocational motion of a single bubble in a fluid, Levich (1962) avoided this difficulty and evaluated the drag on the bubble from the viscous dissipation method. Thus, at steady state, the rate of viscous energy dissipation must equal the work done by the viscous force on the bubble per unit time and therefore

$$\dot{E}_{\mathrm{d}} = \boldsymbol{F}_{\mathrm{v}}^{\alpha} \cdot (\boldsymbol{U} - \boldsymbol{v}^{\alpha}), \tag{22}$$

where $\boldsymbol{F}_{\mathrm{v}}^{\alpha}$ is the viscous force on the bubble and $\dot{E}_{\mathrm{d}}$ is the rate of viscous energy dissipation. Now since the velocity field to leading order is given by the potential flow approximation everywhere in the liquid, a leading-order estimate of the viscous dissipation, and hence the drag, cn be obtained by using the potential flow approximation for the velocity field in the dissipation integral, i.e.

$$\dot{E}_{\mathrm{d}} = \frac{\mu}{2} \int_{\tau_{\mathrm{f}}} \left(\frac{\partial u_i}{\partial x_j} + \frac{\partial u_j}{\partial x_i} \right)^2 \mathrm{d}V = -\mu \int_{S^{\alpha}} \boldsymbol{n} \cdot \nabla |\nabla \phi|^2 \, \mathrm{d}A. \tag{23}$$

Substituting $\phi = \boldsymbol{U} \cdot \boldsymbol{x} - a^{\alpha 3} (\boldsymbol{v}^{\alpha} - \boldsymbol{U}) \cdot \boldsymbol{x} / (2r^3)$ for an isolated bubble in a uniform flow of velocity $\boldsymbol{U}$ at infinity, we obtain the Levich's expression for the drag on the bubble α as

$$\boldsymbol{F}_{\mathrm{v}}^{\alpha} = 12\pi\mu a^{\alpha} (\boldsymbol{U} - \boldsymbol{v}^{\alpha}). \tag{24}$$

In the Levich's calculation the translational velocity was constant. The same result, however, was proven to hold for a time-dependent velocity and small displacements in Prosperetti (1977). Recently, Kang & Leal (1988) proved that (24) gives correctly the instantaneous force on the bubble regardless of the time dependence of the translational velocity.

It is not clear how to extend the above result for an isolated bubble to the case of drag on a bubble in the presence of many other bubbles. The rigorous approach would be to follow the method of Kang & Leal (1988), which, however, presents some technical difficulties that do not arise in the case of a single bubble. More specifically, the expression for the viscous correction to the pressure obtained by Kang & Leal contains certain integrals involving the vorticity distribution. They show that these integrals vanish identically for the case of a single bubble, owing to the symmetry of the flow around the bubble. For the case of many bubbles, however, this symmetry is not preserved and one would then have to evaluate the vorticity distribution around each bubble, a task that is far more difficult.

A commonly used method for estimating drag on a bubble in the presence of other bubbles is to equate the Rayleigh dissipation function to the total energy dissipation. Thus, according to this approximation, the drag force on the bubble α is computed from

$$\boldsymbol{F}_{\mathrm{v}}^{\alpha} = -\tfrac{1}{2}\boldsymbol{\nabla}_{v^{\alpha}}\dot{E}_{\mathrm{d}}, \tag{25}$$

where $\dot{E}_{\mathrm{d}}$ is the rate of energy dissipation in the basic unit cell. As shown in (23), the energy dissipation can be related to the sum of integrals on the surface of all the bubbles in the unit cell, and upon using the expansion of ϕ in surface harmonics around each bubble, it can be shown that $\dot{E}_{\mathrm{d}}$ is given by

$$\dot{E}_{\mathrm{d}} = \mu \sum_{\gamma=1}^{N} \sum_{n=1}^{\infty} \sum_{m=0}^{n} \Lambda_{nm}(D_{nm}^{\gamma 2} + \tilde{D}_{nm}^{\gamma 2})\, a^{\gamma^{-2n-3}}, \tag{26}$$

with

$$\Lambda_{nm} = 4\pi \frac{(1+\delta_{m0})(n+1)(2n+1)(n+m)!}{n(n-m)!}. \tag{27}$$

Thus, the viscous force on the bubble α can be evaluated using

$$F_{\mathrm{v}_i}^{\alpha} = -\mu \sum_{\gamma=1}^{N} \sum_{n=1}^{\infty} \sum_{m=0}^{n} \Lambda_{nm}\, a^{\gamma^{-2n-3}} \left[D_{nm}^{\gamma} \frac{\partial D_{nm}^{\gamma}}{\partial v_i^{\alpha}} + \tilde{D}_{nm}^{\gamma} \frac{\partial \tilde{D}_{nm}^{\gamma}}{\partial v_i^{\alpha}} \right]. \tag{28}$$

Because of the linearity of the governing equation for ϕ, the derivatives can be evaluated by solving a boundary-value problem in which the velocity of all the bubbles except bubble α is zero and requiring that the overall velocity of the mixture is zero (for constant-$\boldsymbol{U}$ simulations). Thus, if there are N bubbles per unit cell, then all the derivatives may be evaluated by solving the N-bubble interaction problem a total of $3N$ times.

The above method of estimating the drag on each individual bubble is time consuming when N is large. We have therefore used another approach for evaluating drag on each bubble as described below. Both methods give essentially the same value of the drag, but one is computationally more efficient. The second method, which we now describe, is based on the exact analysis for small-amplitude oscillatory flows and is described in more detail in Sangani (1991). According to this method, one first solves for the inviscid approximation and determines A_{nm}^{α}, and hence the coefficients D_{nm}^{α}. This potential flow has a correction of $O(Re^{-\frac{1}{2}})$ within a thin region near the surface of the bubble, and this correction in turn modifies the pressure and the velocity field to $O(Re^{-1})$ everywhere including the regions away from the surface of the bubbles. It is this correction of $O(Re^{-1})$ to the pressure that is required in evaluating the drag on the bubble correct to $O(Re^{-1})$. The analysis of the flow in the region close to the surface of the bubbles then results in the following boundary value problem to be solved for the $O(Re^{-1})$ viscous correction ϕ^{v} to the potential. ϕ^{v} satisfies the Laplace equation together with the boundary condition

$$f_{nm}^{\alpha \mathrm{v}'}(a^{\alpha}) = -2(n+1)(2n+1)\, D_{nm}^{\alpha}\, a^{\alpha^{-n-2}}. \tag{29}$$

Here $f_{nm}^{\alpha \mathrm{v}}$ is the coefficient of the surface harmonic Y_{nm} in the expansion of ϕ^{v} around the surface of the bubble α. This coefficient can be expressed as in (11), i.e.

$$f_{nm}^{\alpha \mathrm{v}}(s) = C_{nm}^{\alpha \mathrm{v}}\, s^{n} + D_{nm}^{\alpha \mathrm{v}}\, s^{-n-1}. \tag{30}$$

Substituting (30) into (29), we obtain

$$nC_{nm}^{\alpha \mathrm{v}} - (n+1)\, D_{nm}^{\alpha \mathrm{v}}\, a^{\alpha^{-2n-1}} = -2(n+1)(2n+1)\, D_{nm}^{\alpha}\, a^{\alpha^{-2n-1}}. \tag{31}$$

A similar relation applies to $\tilde{C}_{nm}^{\alpha \mathrm{v}}$ and $\tilde{D}_{nm}^{\alpha \mathrm{v}}$.

Once these coefficients for the viscous correction have been determined, the force on the bubble α is evaluated from

$$F^{\alpha}_{v_1} = 4\pi\mu a^{\alpha^{-2}} D^{\alpha v}_{10}, \tag{32}$$

with similar relations for the components of the viscous force along the x_2 and x_3 axes obtained by replacing $D^{\alpha v}_{10}$ in the above by $-D^{\alpha v}_{11}$ and $-\tilde{D}^{\alpha v}_{11}$ respectively.

The above scheme for estimating the viscous force on individual bubbles is correct to the leading order, $O(1/Re)$, for small-amplitude displacements in small-frequency oscillatory flows. Interestingly, the force on a bubble evaluated in this manner agrees with that computed from the gradient of the dissipation function (cf. (26)) so that the dissipation method is also exact, at least for the special case of small-amplitude, small-frequency oscillatory flows. The main advantage, however, in using the second method outlined here is the considerable saving in computation of the viscous forces on the bubbles. More specifically, the above scheme requires solving a system of equations only once, as opposed to the gradient method which requires solving the system of equations a total of $3N$ times.

A simple calculation for the drag on a bubble in the presence of another bubble at a distance R from it is illustrated in Appendix A, where we also show that the two methods of evaluating drag on individual bubbles give identical results, at least up to $O((a/R)^8)$.

2.3. *Equation of motion for the bubbles*

Once the velocity potential and viscous forces are determined, the next step is to evaluate the trajectories of individual bubbles. Since the bubbles are assumed to have negligible mass, the force balance can be written as

$$-\int_{S^{\alpha}} p\boldsymbol{n}\,\mathrm{d}A + \boldsymbol{F}^{\alpha}_{v} = 0. \tag{33}$$

Here p is computed from the potential flow approximation, and the viscous force $\boldsymbol{F}^{\alpha}_{v}$ is evaluated as described in the previous subsection. The pressure is determined from the Bernoulli equation

$$-p = \rho\left(\frac{\partial\phi}{\partial t} + \tfrac{1}{2}\boldsymbol{u}\cdot\boldsymbol{u} - \boldsymbol{g}\cdot\boldsymbol{x}\right). \tag{34}$$

Evaluation of $\partial\phi/\partial t$ in the above expression is difficult as the direct use of (4) requires knowledge of the time derivatives of the strengths of the multipoles. It is convenient instead to use the local expansion (9) of ϕ around the centre of the bubble α for its evaluation. On noting that ϕ in (9) is a function of $\boldsymbol{s}$ and t, with $\boldsymbol{s} = \boldsymbol{x} - \boldsymbol{x}^{\alpha}(t)$, we have

$$\frac{\partial\phi}{\partial t}(\boldsymbol{x}, t) = \frac{\partial\phi}{\partial t}(\boldsymbol{s}, t) - v^{\alpha}_{i}\frac{\partial\phi}{\partial s_i}(\boldsymbol{s}, t) \tag{35}$$

where we have used $v^{\alpha}_{i} = -\partial s_i/\partial t$. The partial derivative on the left-hand side of (35) is evaluated for constant $\boldsymbol{x}$ whereas that in the first term on the right-hand side is evaluated for constant $\boldsymbol{s}$. Using the above expression for the derivative of ϕ, the force balance now reduces to

$$\frac{\mathrm{d}\boldsymbol{I}^{\alpha}}{\mathrm{d}t} \equiv \dot{\boldsymbol{I}}^{\alpha} = \boldsymbol{F}^{\alpha}_{p} + \boldsymbol{F}^{\alpha}_{v} + \boldsymbol{F}^{\alpha}_{g}, \tag{36}$$

where $\boldsymbol{F}^{\alpha}_{p}$ is the force of potential flow interaction given by

$$\boldsymbol{F}^{\alpha}_{p} = \rho\int_{S^{\alpha}} (\tfrac{1}{2}\boldsymbol{u}\cdot\boldsymbol{u} - \boldsymbol{u}\cdot\boldsymbol{v}^{\alpha})\,\boldsymbol{n}\,\mathrm{d}A, \tag{37}$$

$\boldsymbol{F}_g^\alpha = -\rho\sigma^\alpha \boldsymbol{g}$ is the buoyancy force due to gravity and $\boldsymbol{I}^\alpha$ is the impulse associated with the bubble α (cf. (3)). Now all the quantities on the right-hand side of the (36) can be evaluated, and therefore the force balance on the bubble α gives $\dot{\boldsymbol{I}}^\alpha$. If the initial velocity distribution is prescribed, then $\boldsymbol{I}^\alpha$ can be computed once the velocity potential is determined using (21). The force balance then gives an estimate of the impulse associated with each bubble during the subsequent time step. Thus, the problem for subsequent times is to determine the potential field and hence the velocity of the bubbles given their impulses. An algorithm for numerical simulation of the motion of individual bubbles is given in more detail in §2.5 after we discuss the collision of bubbles in the next subsection. The integral in (37) can be evaluated by means of the following expressions

$$\int_{S^\alpha} \boldsymbol{u}\cdot\boldsymbol{u}n_1 \,\mathrm{d}A = \sum_{n=1}^{\infty}\sum_{m=0}^{n} 2H_{nm}[f_{nm}f_{n+1,m} + \tilde{f}_{nm}\tilde{f}_{n+1,m}], \tag{38}$$

$$\int_{S^\alpha} \boldsymbol{u}\cdot\boldsymbol{u}n_2 \,\mathrm{d}A = \sum_{n=1}^{\infty}\sum_{m=0}^{n} H_{nm}[(n-m)(f_{n,m+1}f_{n+1,m} + \tilde{f}_{n,m+1}\tilde{f}_{n+1,m}) - (n+m+2)(f_{nm}f_{n+1,m+1} + \tilde{f}_{nm}\tilde{f}_{n+1,m+1})], \tag{39}$$

$$\int_{S^\alpha} \boldsymbol{u}\cdot\boldsymbol{u}n_3 \,\mathrm{d}A = \sum_{n=1}^{\infty}\sum_{m=0}^{n} H_{nm}[(n-m)(\tilde{f}_{n,m+1}f_{n+1,m} - f_{n,m+1}\tilde{f}_{n+1,m}) - (n+m+2)(f_{nm}\tilde{f}_{n+1,m+1} - f_{n+1,m+1}\tilde{f}_{nm})], \tag{40}$$

$$\int_{S^\alpha} \boldsymbol{u}\cdot\boldsymbol{v}^\alpha n_1 \,\mathrm{d}A = \frac{8\pi a^\alpha}{5}(v_1^\alpha f_{20} - \tfrac{3}{2}(f_{21}v_2^\alpha + \tilde{f}_{21}v_3^\alpha)), \tag{41}$$

$$\int_{S^\alpha} \boldsymbol{u}\cdot\boldsymbol{v}^\alpha n_2 \,\mathrm{d}A = -\frac{12\pi a^\alpha}{5}(v_1^\alpha f_{21} + \tfrac{1}{3}(f_{20} - 6f_{22})v_2^\alpha - 2\tilde{f}_{22}v_3^\alpha), \tag{42}$$

where

$$H_{nm} = \frac{2\pi n(n+2)(n+m+1)!}{(2n+1)(2n+3)(n-m)!}(1+\delta_{m0}). \tag{43}$$

The integral of $\boldsymbol{u}\cdot\boldsymbol{v}^\alpha n_3$ is obtained by interchanging v_2^α and v_3^α in (42). For brevity, we have omitted the superscript α on the functions f_{nm} etc. It should be noted that with the use of relations such as (17), these functions at $s = a^\alpha$ can be related to D_{nm}^α, and hence by use of (12), to A_{nm}^α.

As shown in Sangani & Didwania (1993), $\boldsymbol{F}_{\mathrm{p}}^\alpha$ can alternatively be determined from

$$\boldsymbol{F}_{\mathrm{p}}^\alpha = 4\pi\rho\sum(-1)^n[A_{nm}^\alpha\Delta_m + \tilde{A}_{nm}^\alpha\tilde{\Delta}_m][A_{kj}^\gamma\Delta_j + \tilde{A}_{kj}^\gamma\tilde{\Delta}_j]\left(\frac{\partial}{\partial x_1}\right)^s \nabla S_1(\boldsymbol{x}^\alpha - \boldsymbol{x}^\gamma), \tag{44}$$

where $s = n-m+k-j$, and the summation is to be carried out over γ (1 to N), n (1 to ∞), m (0 to n), k (1 to ∞), and j (0 to k). For $\alpha = \gamma$, S_1 in (44) must be replaced by its non-singular part.

2.4. *Collision of bubbles*

We now address the question of what happens when two bubbles approach each other. The attractive force between the bubbles is generally caused by the reduction in the pressure in the gap between the two bubbles compared to the ambient pressure. This

force remains finite in the limit of a vanishingly small gap provided that the bubbles remain spherical. The viscous forces are generally small in magnitude at large Reynolds numbers so that they also cannot prevent the bubbles from approaching arbitrarily close to each other. It may be noted that the viscous forces cannot prevent bubbles free of surface-active impurities from approaching each other even when the Reynolds number is very small as shown, for example, by Davis, Schonberg & Rallison (1989). Thus, the viscous forces are unimportant, and the bubbles approach each other with a finite relative velocity. Once the bubbles are close enough, the finite surface tension effects become important but, in the absence of surface-active impurities, they coalesce if the Weber number is small. As mentioned in the Introduction, experimental observations on the dynamics of a pair of bubbles in a large Reynolds number flow have been reported by Kok (1989). He found that the bubbles bounce away from each other almost instantaneously in the presence of surface-active impurities. If the concentration of the impurities is not too large, the observed trajectories of the bubbles are in very good agreement with those obtained theoretically using the potential flow approximation for the fluid velocity together with the viscous drag evaluated from the dissipation method described in the previous subsection. If the concentration of the impurities is moderate or high, a finite-size recirculation region forms behind the bubbles and affects the dynamics of the pair of bubbles, and the potential flow approximation breaks down. In the present study, therefore, we shall consider the case in which the surface-active impurities are present in a small amount so that the potential flow approximation remains valid and at the same time the bubbles do not coalesce. This is perhaps the simplest situation to examine theoretically. As mentioned earlier, Kok (1989) also observed that the bounce of the bubbles is almost instantaneous, and therefore we shall assume the collision of the bubbles to be relatively short-time phenomenon on the timescale of the inertial dynamics.

We now return to the discussion of motion of many bubbles and examine what happens when a pair of bubbles undergoes a collision. Since the timescale for the collision is small and the Reynolds number of the flow is large, we neglect the viscous effects during the collision. The invariants for inviscid interactions are described in detail in Appendix B. In the calculations that follow, we shall take $\boldsymbol{U} = 0$. The results we derive, however, can be shown to be valid even when $\boldsymbol{U}$ is a constant other than zero, or when $\boldsymbol{G}$ is a constant instead of $\boldsymbol{U}$. As shown in the Appendix B, the momentum and kinetic energy of the liquid are related to the sums of $\boldsymbol{I}^\alpha$ and e^α, and that these sums remain invariant. Here, e^α is defined via

$$e^\alpha = \tfrac{1}{2}\boldsymbol{I}^\alpha \cdot \boldsymbol{v}^\alpha \quad (\boldsymbol{U} = 0). \tag{45}$$

The collision of bubbles is different from the collision of perfectly elastic particles in a vacuum in the sense that all the momentum and the energy is contained by the medium in the former case as the bubbles are essentially massless. As we shall see presently, a consequence of this fact is that the velocities of all the bubbles in the dispersion are affected whenever any two bubbles collide. To calculate these velocity changes, let us suppose that bubbles labelled 1 and 2 collide. We may imagine that a very short-range force comes into play when they approach very close to each other and that this force is directed along the separation vector. This force, for example, may result from the repulsion among the molecules of the surface-active impurities adsorbed at the interface, or may arise due to a surface tension gradient-driven motion of the liquid into the gap between the bubbles caused by the depletion of the surface-active impurities there. The exact details of the mechanism by which such a force would arise are not important provided that the collision is a short-timescale process. Thus, on the

inertial timescale, we may suppose that an equal and opposite impulse is applied to the two bubbles and write

$$\frac{\mathrm{d}\boldsymbol{I}^1}{\mathrm{d}t} = F_c\,\delta(t-t_c)\,\boldsymbol{m}_c \tag{46}$$

for time t close to the collision time t_c. Here, F_c is the magnitude of the impulse, and $\boldsymbol{m}_c$ is the unit vector along the separation as given by

$$\boldsymbol{m}_c = \frac{\boldsymbol{x}^1-\boldsymbol{x}^2}{a^1+a^2}, \tag{47}$$

where a^1 and a^2 are the radii of the colliding bubbles. Integrating (47) with time in the immediate vicinity of t_c then leads to a change in the impulse of bubble 1 during the collision process as given by $\Delta\boldsymbol{I}^1 = F_c\,\boldsymbol{m}_c$. The change in the impulse of bubble 2 is equal in magnitude and opposite in the direction, and that of all the other bubbles in the cell is zero. Since the sum of impulses is conserved by this choice of change in impulses, we need only to calculate the change in the sum of e^α. The condition of its invariance will then provide us with an equation for determining the unknown F_c.

The change in velocities of the bubbles during the collision must be linear in F_c and therefore we write

$$2\Delta e^\alpha = \Delta(\boldsymbol{I}^\alpha\cdot\boldsymbol{v}^\alpha) = F_c(\boldsymbol{v}^\alpha\cdot\hat{\boldsymbol{I}}^\alpha+\boldsymbol{I}^\alpha\cdot\hat{\boldsymbol{v}}^\alpha)+F_c^2(\hat{\boldsymbol{v}}^\alpha\cdot\hat{\boldsymbol{I}}^\alpha), \tag{48}$$

where $\hat{\boldsymbol{v}}^\alpha$ is the change in the velocity of bubble α due to unit impulses applied along the separation vector of the colliding pair, and $\boldsymbol{v}^\alpha$ is the velocity before the collision. In other words, we have taken $\Delta\boldsymbol{v}^\alpha = F_c\,\hat{\boldsymbol{v}}^\alpha$. The same convention applies to the impulses also, and in particular we have

$$\hat{\boldsymbol{I}}^1 = -\hat{\boldsymbol{I}}^2 = \boldsymbol{m}_c, \quad \hat{\boldsymbol{I}}^\alpha = 0, \quad \alpha = 3,4,\ldots,N. \tag{49}$$

Now, since the sum of e^α does not change during the collision, (48) yields two values of F_c, one of which equals zero and corresponds to no collision, and the other corresponds to the magnitude of the total impulse during the collision

$$F_c = -\frac{\Sigma(\hat{\boldsymbol{I}}^\alpha\cdot\boldsymbol{v}^\alpha+\hat{\boldsymbol{v}}^\alpha\cdot\boldsymbol{I}^\alpha)}{\Sigma(\hat{\boldsymbol{I}}^\alpha\cdot\hat{\boldsymbol{v}}^\alpha)}, \tag{50}$$

where the summation is over all the bubbles in the unit cell. Thus, in dynamic simulations, we first move the bubbles to the point where they collide and determine $\hat{\boldsymbol{v}}^\alpha$ by solving for the velocity potential $\hat{\phi}$ *given the impulses* $\hat{\boldsymbol{I}}^\alpha$ associated with each bubble (cf. (49)). Substituting for $\hat{\boldsymbol{v}}^\alpha$ in (50) allows us to determine F_c and hence the values of $\boldsymbol{I}^\alpha$ and $\boldsymbol{v}^\alpha$ immediately after the collision process. These values are then used for further trajectory calculations.

There is an equivalent expression for F_c that is slightly more useful in dynamic simulations and this can be derived from the reciprocal theorem for the Laplace equation. Since both ϕ and $\hat{\phi}$ are solutions of the Laplace equation, it is easy to show that

$$\sum_{\alpha=1}^{N}\int_{S^\alpha} n_i\left(\phi\frac{\partial\hat{\phi}}{\partial x_i}-\hat{\phi}\frac{\partial\phi}{\partial x_i}\right)\mathrm{d}A = \int_{\partial\tau} n_i\left(\phi\frac{\partial\hat{\phi}}{\partial x_i}-\hat{\phi}\frac{\partial\phi}{\partial x_i}\right)\mathrm{d}A, \tag{51}$$

where $\partial\tau$ is the surface of the unit cell. Now since ϕ on $\partial\tau$ can be expressed as a sum

of a linearly varying part ($\boldsymbol{G}\cdot\boldsymbol{x}$) and a periodic part (cf. (4)), and similarly $\hat{\phi}$ in terms of $\hat{\boldsymbol{G}}\cdot\boldsymbol{x}$ plus a periodic part, the integral on the right-hand side of (51) simplifies to

$$\int_{\partial\tau} n_i\left(G_j x_j \frac{\partial\hat{\phi}}{\partial x_i} - \hat{G}_j x_j \frac{\partial\phi}{\partial x_i}\right) \mathrm{d}A. \tag{52}$$

By application of a divergence theorem and using appropriate expressions for G_j and $\hat{G}_j$ (cf. (4) and (8)), the above integral further simplifies to $\tau G_j \hat{U}_j$, which vanishes since $\hat{U}_j = 0$. Upon substituting zero for the right-hand side of (51), using $\boldsymbol{n}\cdot\nabla\phi = \boldsymbol{n}\cdot\boldsymbol{v}^\alpha$ and the definition of the impulse, we obtain

$$\sum_{\alpha=1}^{N} I_i^\alpha \hat{v}_i^\alpha = \sum_{\alpha=1}^{N} \hat{I}_i^\alpha v_i^\alpha. \tag{53}$$

Substituting this result into (50), we obtain another expression for F_c:

$$F_c = -\frac{2\sum_{\alpha=1}^{N}(\hat{\boldsymbol{I}}^\alpha\cdot\boldsymbol{v}^\alpha)}{\sum_{\alpha=1}^{N}(\hat{\boldsymbol{I}}^\alpha\cdot\hat{\boldsymbol{v}}^\alpha)} = -\frac{2\boldsymbol{m}_c\cdot(\boldsymbol{v}^1-\boldsymbol{v}^2)}{\boldsymbol{m}_c\cdot(\hat{\boldsymbol{v}}^1-\hat{\boldsymbol{v}}^2)}, \tag{54}$$

where we have utilized the fact that $\hat{\boldsymbol{I}}^\alpha$ is non-zero only for the colliding pair. It can now be easily seen from the above expression for F_c that the normal component of the relative velocity of bubble 1, with respect to bubble 2, is simply reversed upon collision since the normal component of the relative motion after the collision equals

$$[(\boldsymbol{v}^1 + F_c\,\hat{\boldsymbol{v}}^1) - (\boldsymbol{v}^2 + F_c\,\hat{\boldsymbol{v}}^2)]\cdot\boldsymbol{m}_c, \tag{55}$$

which upon substituting for F_c from (54) reduces to $-\boldsymbol{m}_c\cdot(\boldsymbol{v}^1-\boldsymbol{v}^2)$. It may be noted that this result is valid even when the radii of the colliding bubbles are not equal.

Although the two expressions for F_c derived here are equivalent, there is an important advantage in using (54) in computing the velocities of the bubbles just after the collision as this ensures that the normal component of the relative velocity of the colliding bubbles will reverse upon collision. The computations are usually carried out with a finite number of multipoles in the solution for ϕ and $\hat{\phi}$ and therefore, in general, F_c computed from the two expressions may differ slightly by an amount that depends on the number of multipoles retained. In most instances this difference is unimportant, and, in fact, our earlier calculations were made using (50). However, for some simulations, after carrying out the dynamic simulation for long times when the planar aggregates were nearly formed, we would find that the colliding pair did not reverse its normal component of the relative velocity, and consequently further calculations could not be made. This generally happened when the magnitude of the relative velocity was very small. Therefore, all results presented here were obtained using the second expression for F_c.

2.5. *Algorithms for trajectory calculations*

At time $t = 0$, we start with the prescribed spatial and velocity distribution of the bubbles and determine the potential field by solving for the strength of the multipoles in (4). Once the multipoles are determined, the viscous force is estimated from the method described in §2.2. This requires solving for the viscous correction ϕ_v, which satisfies the Laplace equation, together with the boundary condition on the bubbles determined from the potential flow solution (cf. (29)). The multipoles for this viscous

correction are determined in the same manner as for the potential flow problem. With the viscous force evaluated from relations such as (32), and using the formulae (38)–(42) to evaluate $\boldsymbol{F}_{\mathrm{p}}^{\alpha}$, we determine $\dot{I}_i^{\alpha}$ for each bubble. We also determine I_i^{α} from the potential flow solution with the use of (20) and (21). Next, an Euler scheme is used to estimate the positions and impulses of the bubbles at time $t = \Delta t$. Thus,

$$I_i^{\alpha *}(\Delta t) = I_i^{\alpha}(0) + \Delta t \dot{I}_i^{\alpha}(0) \tag{56}$$

and

$$x_i^{\alpha *}(\Delta t) = x_i^{\alpha}(0) + \Delta t v_i^{\alpha}(0). \tag{57}$$

Here the time step Δt for the integration is determined as follows. First, with (57) giving for the position of bubbles at subsequent times, the minimum time for the collision between any two pairs of bubbles is determined. Next, if this time is greater than the specified time h for integration, then Δt is chosen to equal h. Otherwise, the minimum time for the collision is chosen as Δt.

At the next time step we solve for the potential and viscous flow corrections with the impulses of the bubbles specified as the boundary conditions. The solution in turn allows us to determine the velocity of all the bubbles at time Δt, and this procedure is repeated a number of times to determine the trajectories of all the bubbles. The difficulty with this simple scheme, however, is that it is not very accurate. For the special case of inviscid interaction, the sum of I_i^{α} and e^{α} over all the bubbles must remain invariant, and we use this as a criterion for assessing the accuracy of the integration scheme. Actually, there are a number of variables in the simulations to be selected. These are the number of multipoles retained in the solution (4), the maximum time step h, and the integration scheme. It turned out that the results are not very sensitive to the number of multipoles. In view of the rather large computational efforts involved in these simulations, it is necessary to choose h that is not too small. We found that the sum of I_i^{α} and e^{α} increased slowly with time if we used the scheme described above so that, after a few thousand time steps, the sum of e^{α} increased by as much as 50%. This increase could be substantially decreased for the same value of h by choosing the modified Euler scheme for integration described below.

According to this modified scheme, we use the estimates of the impulses and positions of the bubbles to determine the potential flow field, and hence the velocities of the bubbles, at time $t = \Delta t$. Next, we estimate the average velocities of the bubbles during the time interval and use them to estimate the position of the bubbles at time $t = \Delta t^*$, i.e.

$$x_i^{\alpha}(\Delta t^*) = x_i^{\alpha}(0) + \Delta t^* \tfrac{1}{2}(v_i(0) + v_i^*(\Delta t)) \tag{58}$$

Here Δt^* is the minimum of h and the minimum time for the collision to occur for any pair of bubbles with the modified estimates of the velocities of the bubbles. A similar expression is used to obtain a new estimate of I_i^{α} at time Δt^*. This modified scheme was used for dynamic simulations in the presence of viscous and gravitational forces. For pure inertial interaction calculations, we found that this scheme resulted in a 5–10% increase in the sum of I_i^{α} values and e^{α} values for every 2000 time steps. Since this increase can have a significant effect on the microstructure at long times, a further modification was made to the above scheme for the special case of inertial interactions.

Generally, the sum of impulses changes by less than 0.01% per time step owing to the slight inaccuracy introduced by evaluating the velocity potential using a finite number of multipoles and due to the time discretization. Thus, at the end of every time step, the sum of $\dot{I}_i^{\alpha}$ was evaluated, and this quantity divided by N was subtracted from each of the $\dot{I}_i^{\alpha}$. This difference is indeed an insignificantly small quantity for each time

step, but it ensures that the sum of I_i^α remains unchanged during the simulation. It is difficult, on the other hand, to ensure that the sum of e^α remain invariant throughout the simulation. Therefore, we employed a slightly arbitrary scheme which maintains the sum of this quantity to fluctuate within 2% throughout the simulation. According to this scheme, the sum of e^α was evaluated after every 100 time steps, and if it was greater than its value at time $t = 0$, then the spread of each I_i^α from the mean impulse was reduced arbitrarily by 0.5%. This maintains the sum of I_i^α unchanged and at the same time decreases the sum of e^α (by an amount that can not be estimated *a priori*). It turned out that the sum of e^α was not always greater than its initial value, and so this operation of arbitrarily reducing the spread in the impulses of the bubbles was carried out roughly every 300 time steps. We carried out some simulations with smaller h, for which the accuracy is better, to check that this scheme of arbitrarily reducing the variance in I^α did not produce any significant change in the results.

3. Results

Figure 1 shows various coefficients as functions of the highest order of multipoles N_s retained in solving (4) (i.e. with $n \leqslant N_s$) for $\beta = 0.3$ and for 16 bubbles per unit cell. These results are calculated for a random configuration of bubbles with equal velocities. The total number of unknowns in determining the velocity potential ϕ equals $N_s(N_s+2)N$, where N is the number of bubbles per unit cell. $N_s = 1$ corresponds to obtaining a solution for ϕ by including only the dipoles in (4), whereas $N_s = 5$ corresponds to including up to 2^5 multipoles. The added-mass coefficient C_a, the viscous-drag coefficient C_d, and the energy coefficient E are defined via

$$\langle I_1 \rangle = \frac{1}{N}\sum_{\alpha=1}^{N} I_1^\alpha = \rho\frac{4\pi a^3}{3}[\tfrac{1}{2}C_a(V_1 - U_1) - U_1], \tag{59}$$

$$\langle F_{v_1} \rangle = 12\pi\mu a C_d(U_1 - V_1), \tag{60}$$

$$\langle e \rangle = \tfrac{1}{2}\langle \boldsymbol{I}\cdot\boldsymbol{v} \rangle = \rho\frac{4\pi a^3}{3}|\boldsymbol{V}-\boldsymbol{U}|^2 E, \tag{61}$$

where the x_1-axis is taken in the direction of the buoyancy force and $\boldsymbol{V}$ is the mean velocity of the bubbles. As seen in figure 1, these coefficients change by less than 5% as N_s is increased from 1 to 5. The effect of changing N and N_s on dynamic simulation results for C_a is shown in figure 2. The average velocity of the gas phase is continuously changing and, in computing C_a as a function of time from (59), we used the mean velocity of the bubbles evaluated at that instant. The Reynolds number is defined by

$$Re = \rho a V^*/\mu \quad \text{with} \quad V^* = a^2\rho g/9\mu. \tag{62}$$

The time is non-dimensionalized with a/V^*, and the time step h for integration was chosen to be 0.02. The results shown in figure 2 were obtained by averaging C_a over 300 time steps. As seen in this figure, the fluctuations in C_a are substantial and that the differences in the dynamic behaviour for different N_s and N at given t are relatively small.

Calculations for C_a and C_d for β ranging from 0.1 to 0.5 showed that these coefficients continued to increase with time, with the most pronounced increase occurring for lower values of β. For example, for $\beta = 0.1$, C_a increased from about 1.3 at $t = 0$ to 4 at $t = 100$. The reason for this marked increase in C_a or C_d can be

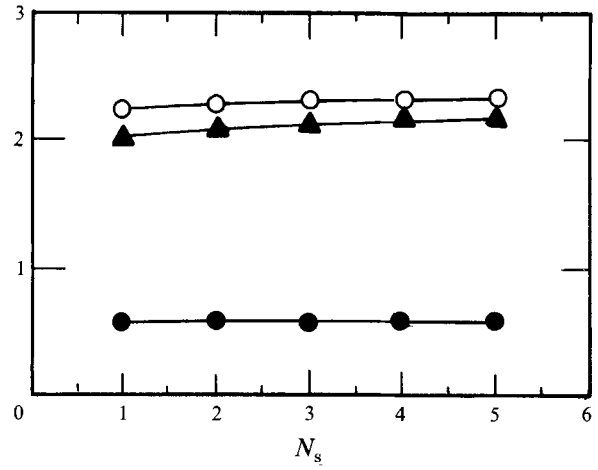

FIGURE 1. Convergence of the numerical results for the added-mass coefficient C_a (○), the viscous-drag coefficient C_d (▲), and the energy coefficient E (●) as a function of the highest-order N_s of singularities retained in the solution. Here, $\beta = 0.3$, $N = 16$, and the velocities of the bubbles are equal.

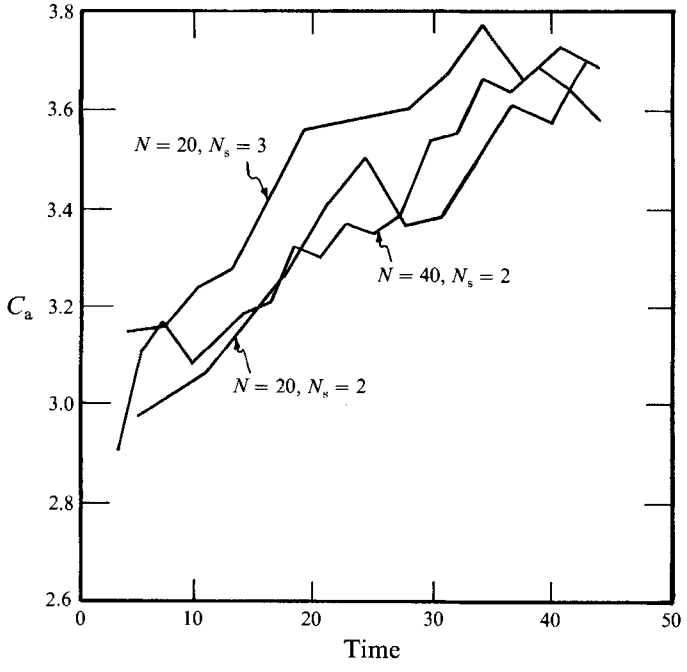

FIGURE 2. The added mass coefficient as a function of time for three different combinations of N and N_s. $Re = 500$, $\beta = 0.3$.

understood by examining the microstructure as a function of time. As seen in figure 3, the bubbles arrange themselves in a horizontal plane as the time progresses. These calculations were made with $N = 20$, $N_s = 2$, and $Re = 500$. The formation of planar aggregates is not dependent on N or N_s. This was verified by repeating calculations with $N_s = 3$ and $N = 16$ and with $N_s = 2$ and $N = 40$. The latter case is shown in figure 4. Here, all the bubbles in the cell cannot be packed into one planar aggregate, and,

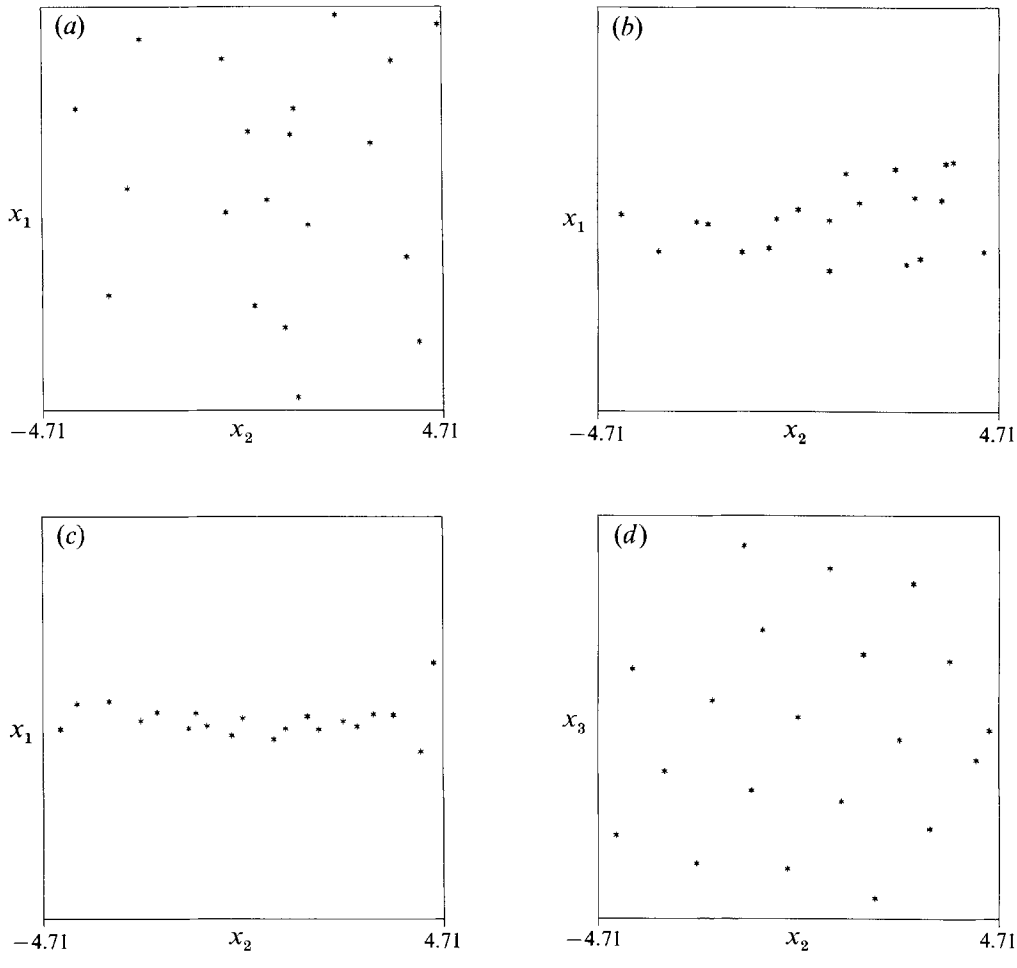

FIGURE 3. The spatial configuration of bubbles at different times for $\beta = 0.1$, $Re = 200$, and $N = 20$. (*a*) $t = 0$; (*b*) $t = 33$; (*c*, *d*) $t = 60$.

therefore, two aggregates form. To distinguish the bubbles in the aggregate near the plane $x_1 = 0$ from the others, we have denoted their centres by pluses. It is interesting to note that this aggregate contains the same number of bubbles (21) as t varies from 37 to 105. The aggregate near $x_1 = 0$ is finite in the x_2-direction but extends the full length of the unit cell in the x_3-direction, while the other aggregate extends fully in the x_2-direction.

The planar aggregates form even when the initial velocity distribution is highly non-uniform. For example, we repeated the calculations for $N = 20$ with an initial velocity given by $v_i^\alpha = \xi_i^\alpha$, ξ_i^α being a uniform random variable between -0.5 and 0.5. The planar aggregates formed in this case in roughly the same amount of time ($t < 70$). The magnitude of Re also played a relatively minor role; it only changed the time it took to form planar aggregates. The results for C_a as a function of time for three different Re and an initial random velocity distribution are shown in figure 5. The planar aggregates were seen for $Re = 100$ by $t = 30$ and for $Re = 500$ and 2000 by $t = 60$ and 120, respectively. These estimates of times are only approximate, and no scaling of the time of aggregate formation with Re is implied. Of course, if $Re = \infty$, then the

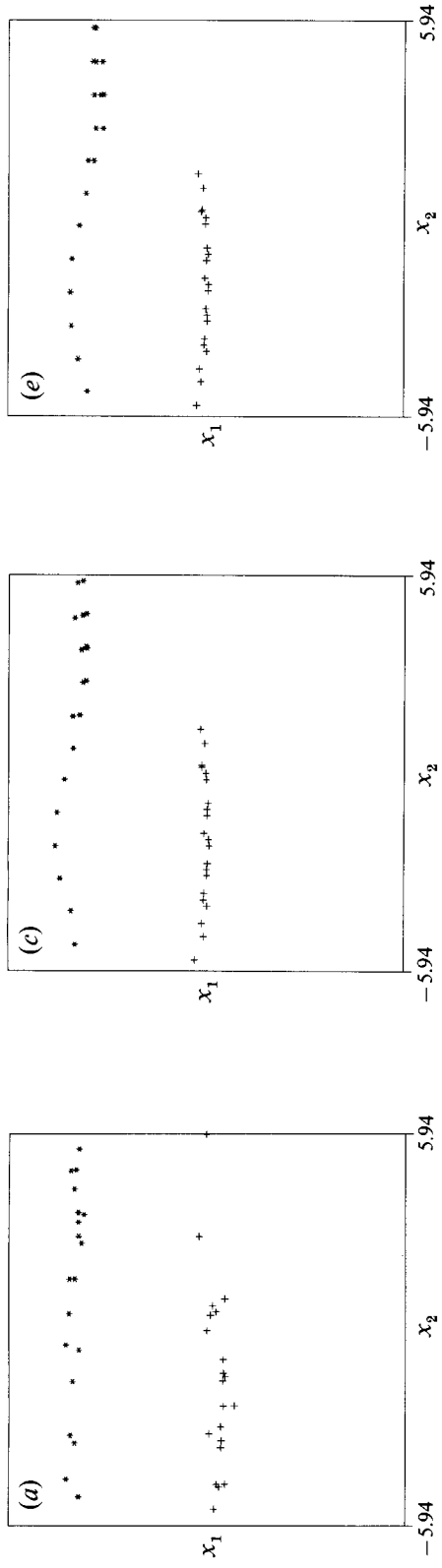

FIGURE 4. The spatial configuration of bubbles at different times for $N = 40$, $\beta = 0.1$, and $Re = 200$. The bubbles near the plane $x_1 = 0$ are denoted by pluses and the others by stars. (*a*) $t = 37$; (*b*) $t = 61$; (*c*, *d*) $t = 90$; (*e*, *f*) $t = 105$.

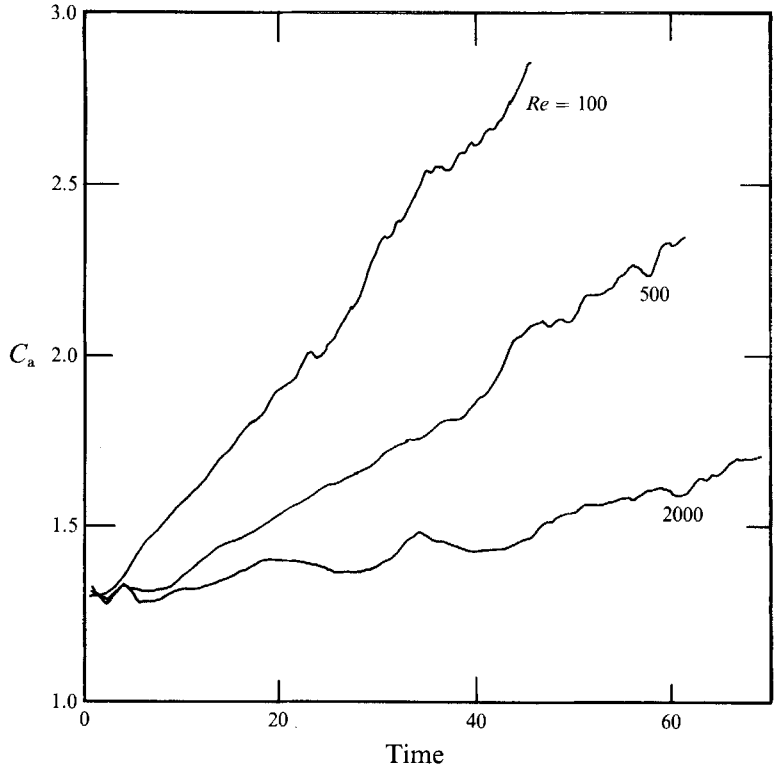

FIGURE 5. The added-mass coefficient C_a as a function of time for three different Reynolds numbers. $\beta = 0.1$ and $N = 20$.

microstructure at long times continues to depend on the initial velocity (or impulse) distribution. In that case, the sums of I^α and $e^\alpha = \frac{1}{2}(I^\alpha \cdot v^\alpha)$, which depend on initial spatial and velocity distributions, remain constant throughout the simulation. Figure 6 shows results for two different initial conditions. In one case the initial impulse distribution is uniform ($I_i^\alpha = \delta_{i1}$) and in the other non-uniform ($I_i^\alpha = \delta_{i1} + \xi_i^\alpha$). In these simulations, the sum of e^α normalized by the average impulse, i.e. $E' = \langle e \rangle (4\pi a^3 \rho/3)/\langle I_1 \rangle^2$, remains constant. We see that the bubbles do not form planar aggregates in these cases. The corresponding results for C_a as a function of time are shown in figure 7. The increase in C_a with time is much smaller in this case than that obtained with finite *Re*. Thus, while the tendency to form planar aggregates results primarily from the inertial interactions, the dissipative mechanism is essential for these aggregates to form.

The average velocity of the mixture was taken to be zero in the results described above. To make sure that the principal finding, i.e. the formation of aggregates, does not depend on this restriction, we also carried out simulations in which $\boldsymbol{G}$ (cf. (8)) was held constant during the simulation. This corresponds to the case in which the average velocity of the liquid remains constant. Once again, we found that the planar aggregates form for finite *Re*. The results that now follow were in fact obtained by taking $G = 0$.

Obvious questions that arise from the results presented here are: (i) what influence, if any, does the artificially imposed periodicity have on the formation of these aggregates; and (ii) whether such aggregates would form if N were much larger. To

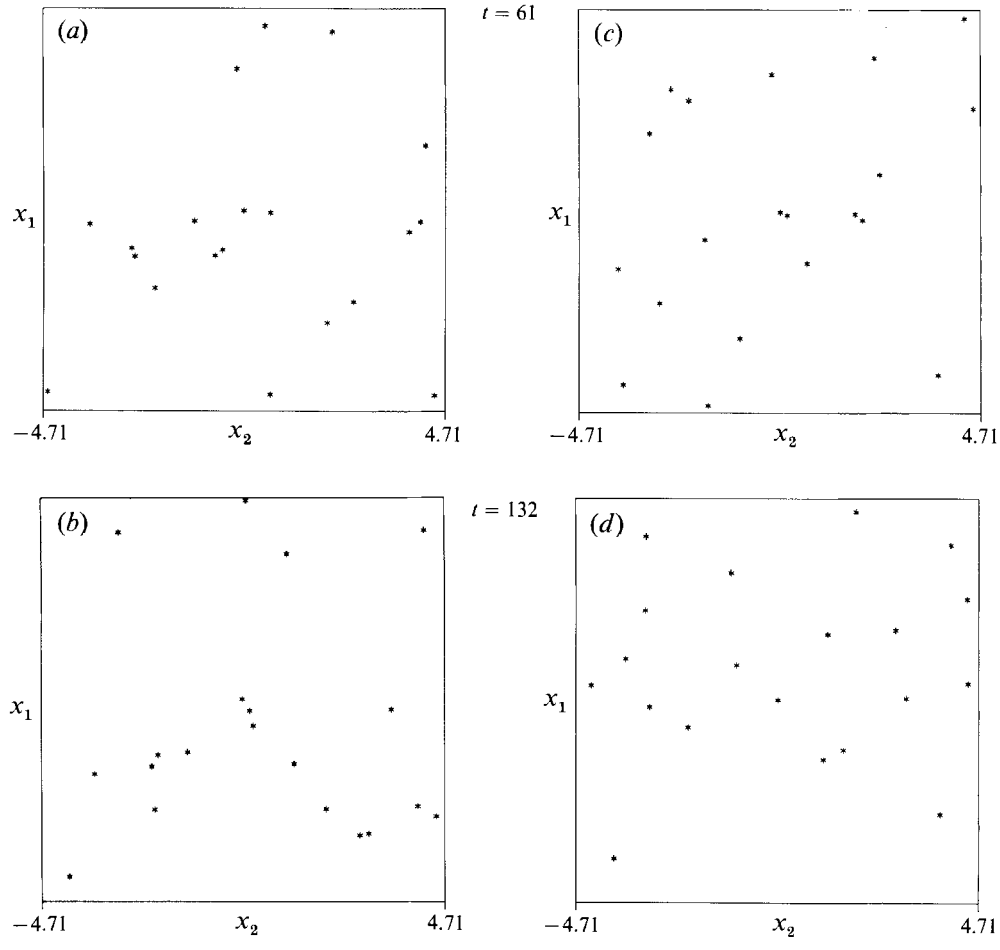

FIGURE 6. The spatial configurations of bubbles at different times for two different initial impulse distribution. $Re = \infty$, $\beta = 0.1$, and $N = 20$. (*a*, *b*) $E' = 0.40$; (*c*, *d*) $E' = 0.50$.

answer the first question, we carried out simulations for a swarm of bubbles, initially cubic in shape, rising through a liquid quiescent at infinity. The calculations for this case are the same as that for N bubbles in a periodic array except that the Green's function $S_1(\boldsymbol{x})$ in (4) is now replaced by $1/|\boldsymbol{x}|$, the Green's function for the infinite space. Also, since the microstructure does not seem to depend on N_s significantly, the calculations for larger N were made with $N_s = 1$. Note that to obtain a non-zero estimate of the potential interaction force $\boldsymbol{F}_p^\alpha$ by the expressions given by (38)–(42), we must use $N_s \geqslant 2$. On the other hand, a non-zero estimate can be obtained even with $N_s = 1$ if we use (44). A detailed comparison of the results obtained by using (44) and $N_s = 1$ with those obtained from (38)–(42) and $N_s = 2$ showed that while the difference in $\boldsymbol{F}_p^\alpha$ for individual bubbles can be anywhere from 0 to 40%, the added mass coefficient calculated by the two methods agreed within few percent. Also, the planar aggregates formed regardless of the choice of N_s and the method of computing $\boldsymbol{F}_p^\alpha$. Therefore, the calculations for larger N to be presented next were made using (44) and $N_s = 1$. The CPU time on an IBM 3090 for a swarm of 150 bubbles with $N_s = 1$ was about 0.5 s per time step, and about 2 s for 120 bubbles in a periodic array. As the bubbles begin

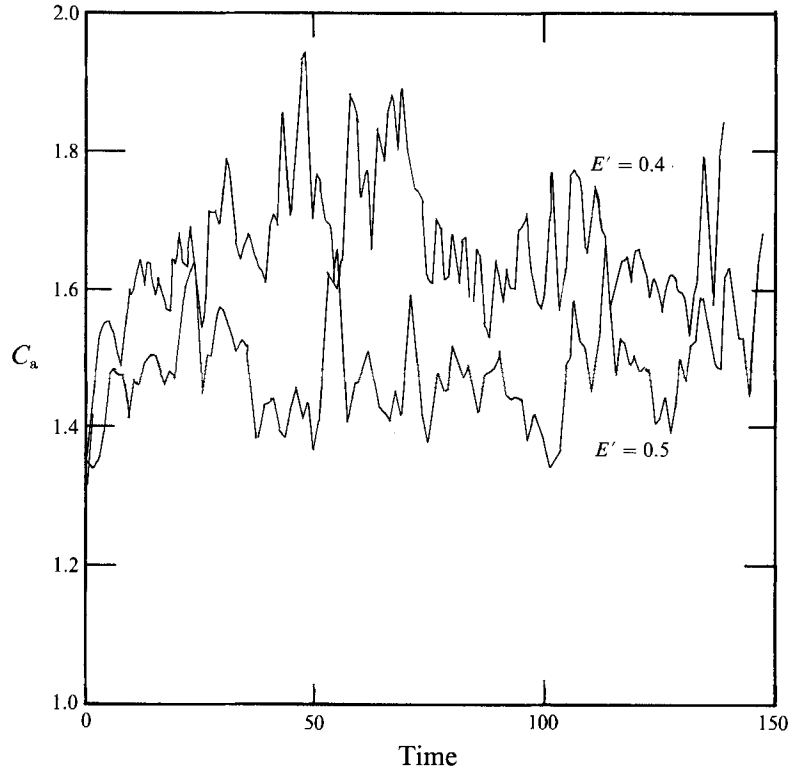

FIGURE 7. The added-mass coefficient C_a as a function of time for the same conditions as in figure 6.

to form aggregates, the time step for any pair of bubbles to collide decreases considerably with the increase in N. Therefore, to carry out simulations to $t = 80$, we typically needed 20 to 40 thousand time steps.

The results for the cubic swarm of bubbles with $N = 150$ are shown in figure 8. At $t = 0$, the bubbles are placed randomly within a cube of size 18.5 units, the radius of the bubbles being unity. This corresponds to $\beta = 0.1$ within the swarm. As seen in figure 8, at $t = 80$, the bubbles have arranged themselves into two large planar aggregates. These aggregates are about 23×23 in size, suggesting the stability of these aggregates over lengths that are significantly larger than the radii of the bubbles.

Returning now to the case of bubbles in periodic arrays, we present in figure 9 the results obtained with $N = 120$ and $\beta = 0.1$. For this situation, and that considered earlier in figure 4, all the bubbles within the cell cannot be packed into a single plane, and the natural question that arises is whether all the bubbles in the cell will eventually form a tightly packed slab that is thicker than the diameter of the bubbles or will there be two or more distinct planar aggregates. As seen in figure 9, the bubbles very quickly arrange themselves into two planes. The change in the microstructure from $t = 60$ to 110 is relatively small. At $t = 74$, roughly 64 bubbles are in one aggregate and 56 in the other, and at $t = 110$, the larger aggregate contains 67 bubbles. From this calculation, however, it is difficult to establish the behaviour at $t = \infty$. A possible scenario is that the aggregate with the smaller number of bubbles will loose one bubble at a time and the other one gain it such that eventually all the bubbles will pack into a single, thicker slab. The other possible scenario is that the two slabs will have exactly the same

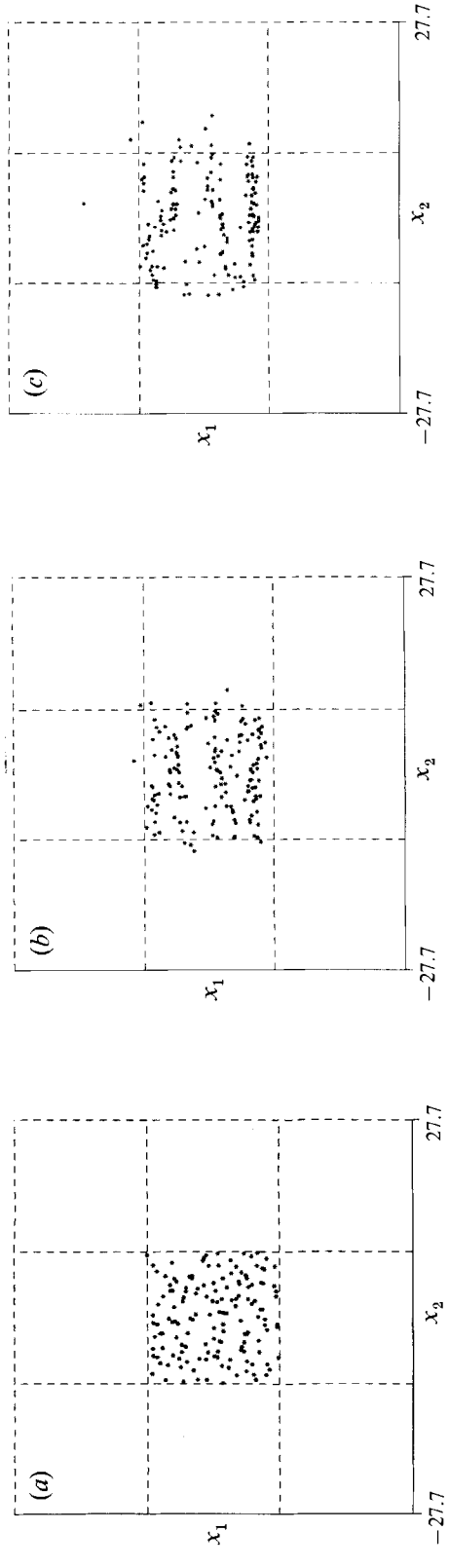

FIGURE 8. The spatial configurations of a swarm of 150 bubbles initially placed within a cube of size 18.5 units. The radius of bubbles is unity and $Re = 200$. (*a*) $t = 0$, (*b*) $t = 13$, (*c*) $t = 25$, (*d*) $t = 42$, (*e*) $t = 61$, (*f*) $t = 80$.

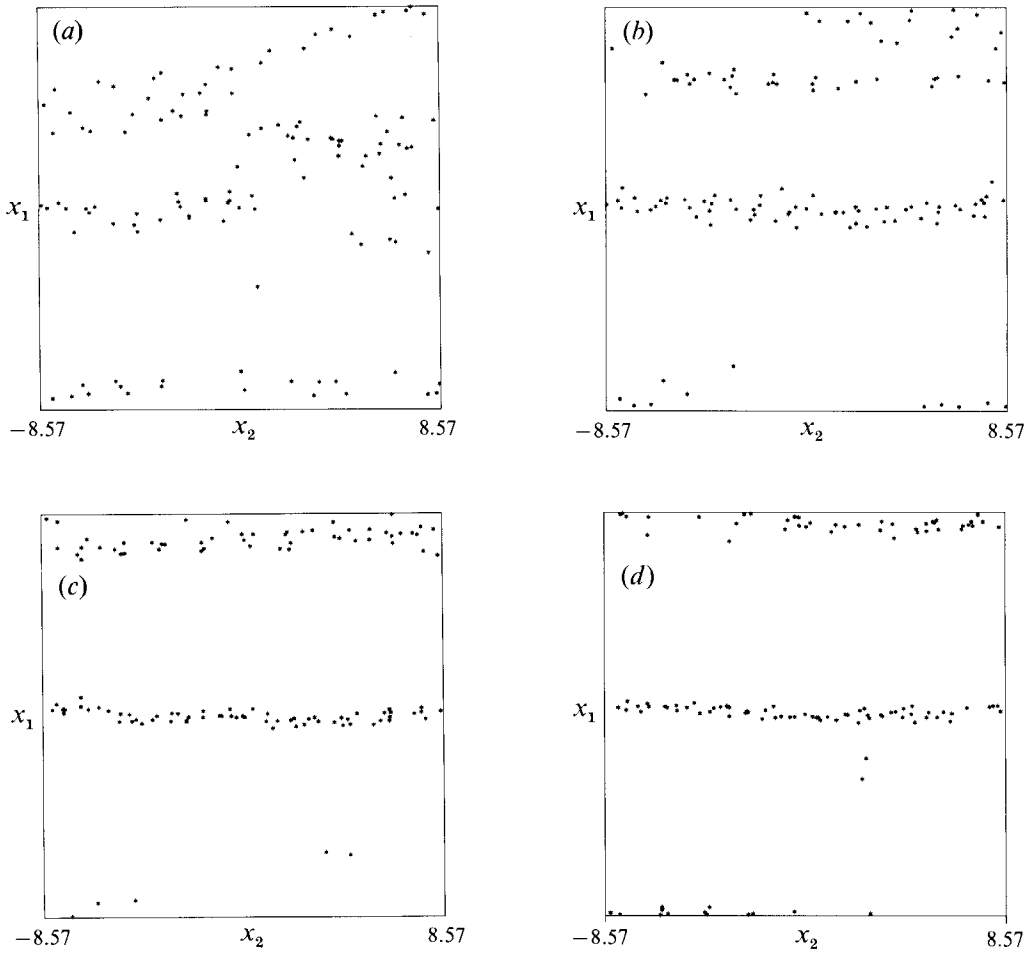

FIGURE 9. The spatial configurations for $N = 120$, $Re = 200$, $\beta = 0.1$. (*a*) $t = 37$, (*b*) $t = 61$, (*c*) $t = 76$, (*d*) $t = 110$.

number of bubbles and will therefore move with the same velocity. Unfortunately, the computational effort involved in pursuing this question is excessive, and therefore we are unable to answer it. At any rate, the results presented in this section amply suggest that the state of monodispersed uniform bubbly liquids is unstable, and that the planar aggregates formed as a result are stable up to fairly large sizes.

In polydispersed liquids, bubbles of different radii are acted upon by significantly different buoyancy forces, and, therefore, it is possible that the aggregates seen above may not form. To test this hypothesis, we first carried out calculations with $N = 40$, $\beta = 0.1$, and $a^\alpha = a(1+\xi^\alpha)$, with ξ^α a uniform random variable between -0.2 to 0.2. We shall refer to such a mixture as 40% polydispersed. We found that a planar aggregate formed within each unit cell even in this case in roughly the same amount of time ($t < 70$) as the corrsponding monodispersed liquid. To see if such aggregates break up if the polydispersivity is larger and β is smaller, we carried out simulations with a 70% polydispersed mixture with $\beta = 0.03$ and with a random initial velocity distribution with a zero mean. Note that the terminal rise velocity of a bubble with radius $1.35a$ is roughly 4.3 times that of a bubble with radius $0.65a$. The results of simulations with $N = 60$ and $Re = 200$ are shown in figure 10. Once again, we see that

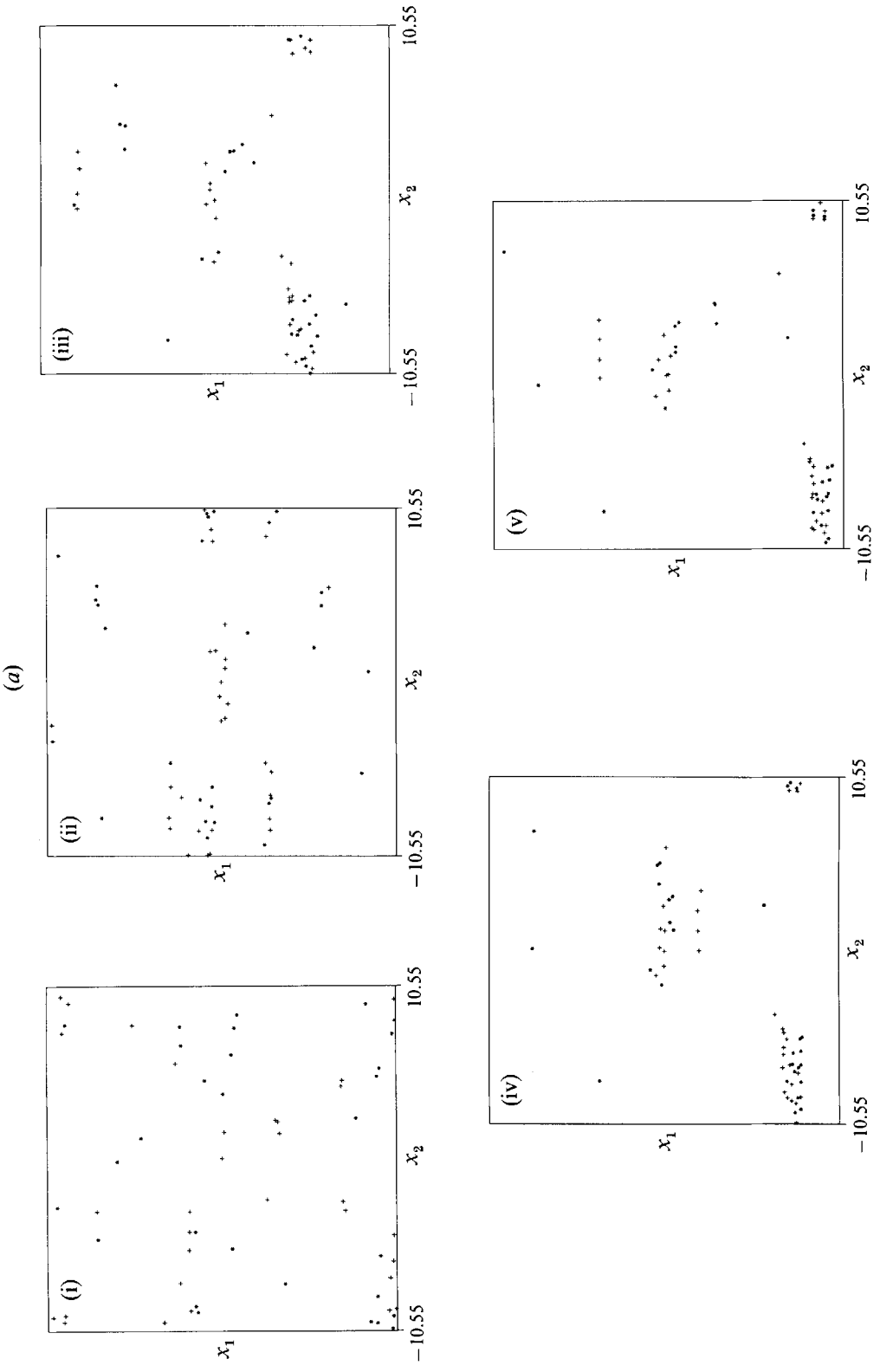
(a)
(i)
(ii)
(iii)
(iv)
(v)
x_1
x_2
10.55
−10.55

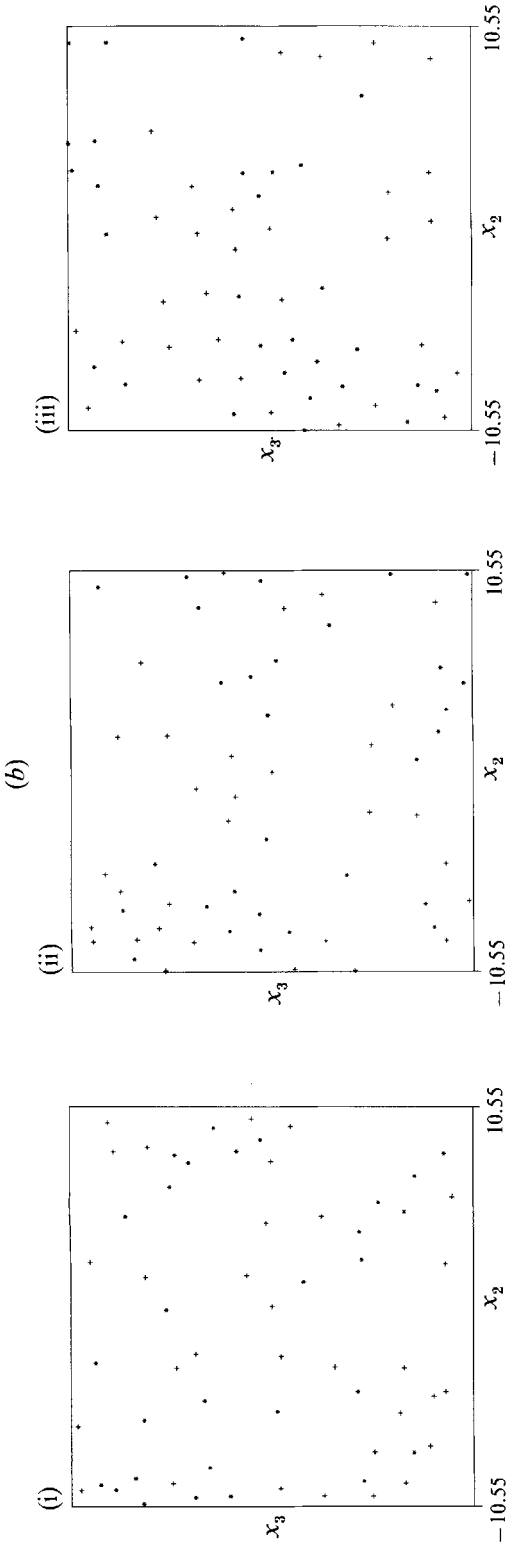

FIGURE 10. The spatial configurations for a 70% polydispersed liquid with $\beta = 0.03$, $Re = 500$, and $N = 60$. The centres of bubbles with radius greater than unity are denoted by pluses and the others by stars: (*a*) the front views; (*b*) the top views. (i) $t = 40$, (ii) $t = 73$, (iii) $t = 107$, (iv) $t = 134$, (v) $t = 151$.

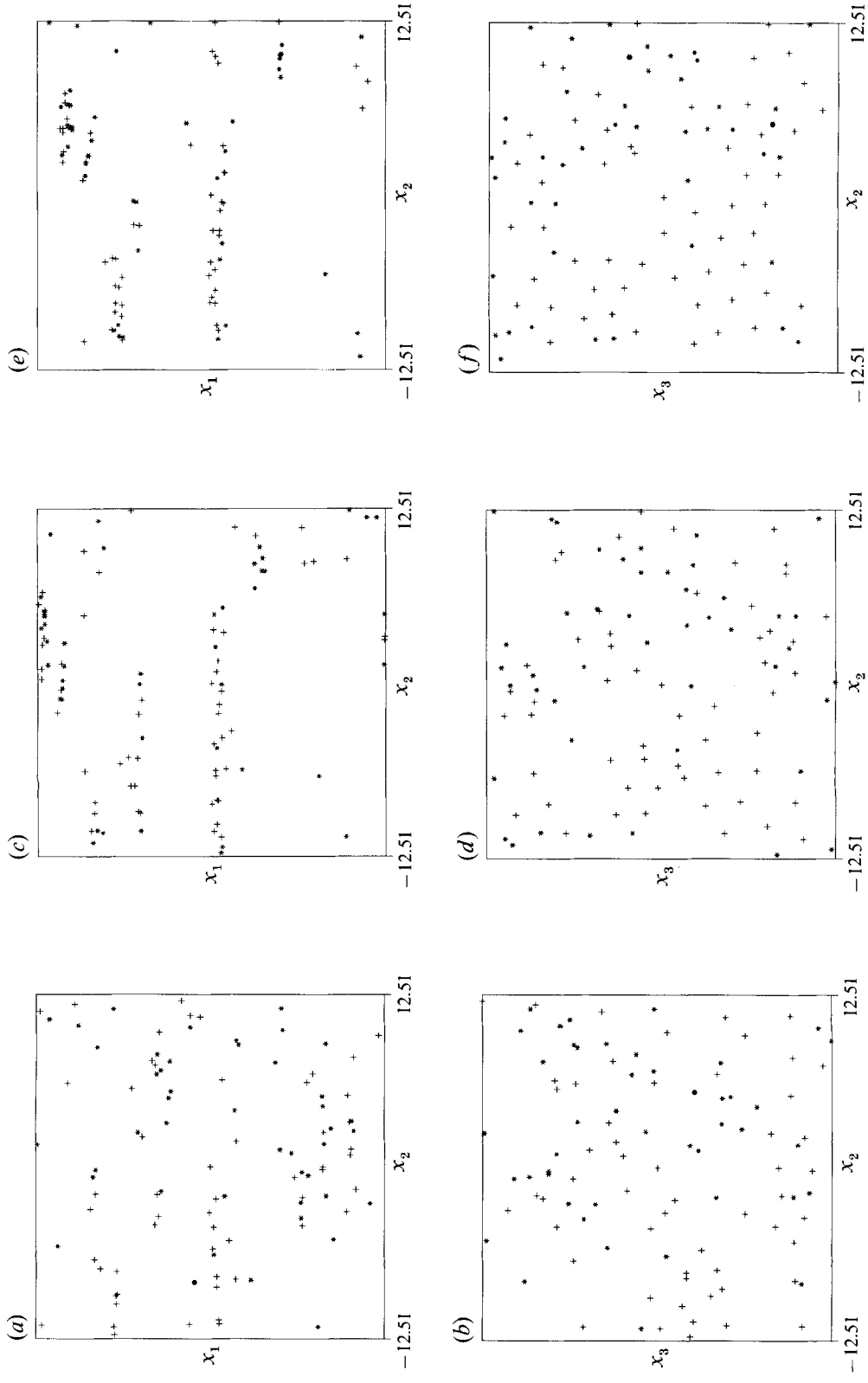

FIGURE 11. As figure 10 but for $N = 100$. (a, b) $t = 42$; (c, d) $t = 63$; (e, f) $t = 80$.

the state of uniform random bubbly liquid is unstable. Unlike the results presented earlier, however, it appears that we do not see planar aggregates extending over the complete cross-section of the unit cell. Rather, it appears that there are two or three distinct aggregates moving with different speeds through the liquid. Whether this phenomenon, i.e. formation of aggregates smaller than the size of the unit cell, depends on the amount of polydispersivity and β or N can be examined by carrying out simulations with larger N. Such results are shown in figure 11, The initial conditions for the simulation are same as in the previous case, but now $N = 100$. The larger number of bubbles allows larger aggregates to form, and thus we believe that large aggregates will form even in polydispersed liquids provided that we choose sufficiently large N.

4. Concluding remarks

We have shown that the uniform spatial distribution of bubbles is unstable and that planar aggregates form as a result. These aggregates form even when the size distribution of the bubbles is non-uniform, and they are stable up to fairly large sizes.

It is possible that the model we have used here for the flow past bubbles at large but finite Reynolds number is oversimplified by assuming that the flow is essentially irrotational. The assumption of the potential or irrotational flow may be justified in case of a single bubble or pair of bubbles rising in otherwise quiescent liquid but not for non-dilute dispersions of bubbly liquids. At any rate, the calculations presented here suggest that we shall need to invoke a further hypothesis about the nature of the forces that keep the bubbles from forming aggregates. One possibility is that there is a random distribution of vorticity in the dispersion that is caused by the flow around bubbles and at the wall of the container in which the dispersion is flowing. It may be possible to model this distribution as giving rise to an additional random force on the bubbles. Another possibility is that a macroscopic flow generated due to the bubble distributor at the bottom of the vessel may induce a shear flow or stirring sufficient to prevent the aggregates from forming. Finally, we have assumed here that the bubbles remain spherical. This requires that the radii of bubbles be smaller than 1 mm. Most experimental observations, however, are made with bubbles of larger radii. Further investigation is needed for determining which of these factors is responsible for the discrepancy between the experiments and the model used here.

This work has been supported by the US Department of Energy, Office of Basic Energy Sciences, under Grant No. DE-FG02-90ER14136 and by the National Science Foundation under Grant No. CBT-8800451. The authors are grateful to Professors D. L. Koch and A. Prosperetti for valuable discussions. The authors also acknowledge the use of supercomputer facilities at the Cornell Theory Center.

Appendix A. Viscous forces on a pair of bubbles

We illustrate in more detail in this appendix how the viscous forces on the bubbles are evaluated by considering the simple case of axisymmetric motion of two bubbles, labelled 1 and 2, with their respective positions at $\boldsymbol{x}^1 = \frac{1}{2}\boldsymbol{e}_1 R$ and $\boldsymbol{x}^2 = -\frac{1}{2}\boldsymbol{e}_1 R$, and velocities along the x_1-axis of V_1 and V_2. Here, $\boldsymbol{e}_1$ is the unit vector along the x_1-axis. The radii of the bubbles will be taken to be unity. The velocity potential is given by

$$\phi = \sum_{n=1}^{\infty} \sum_{\alpha=1}^{2} A_n^{\alpha} \frac{(-1)^n}{n!} \left(\frac{\partial}{\partial x_1}\right)^n \frac{1}{|\boldsymbol{x} - \boldsymbol{x}^{\alpha}|}. \tag{A 1}$$

The strengths of multipoles A_n^α can be determined from the boundary condition on the surface of the bubbles in a straightforward manner to yield

$$A_1^1 = -\tfrac{1}{2}V_1 + \tfrac{1}{2}V_2 R^{-3} - \tfrac{1}{2}V_1 R^{-6} - \tfrac{3}{2}V_1 R^{-8} + O(R^{-9}), \tag{A 2}$$

$$A_1^2 = -\tfrac{1}{2}V_2 + \tfrac{1}{2}V_1 R^{-3} - \tfrac{1}{2}V_2 R^{-6} - \tfrac{3}{2}V_2 R^{-8} + O(R^{-9}), \tag{A 3}$$

$$A_2^1 = -V_2 R^{-4} + V_1 R^{-7} + O(R^{-9}), \tag{A 4}$$

$$A_2^2 = V_1 R^{-4} - V_2 R^{-7} + O(R^{-9}). \tag{A 5}$$

Now the viscous force on each bubble can be evaluated from the dissipation method by use of (28) which yields, on noting that $D_{n0}^\alpha = A_n^\alpha$,

$$-\frac{F_{\rm v}^\alpha}{12\pi\mu} = \sum_{\gamma=1}^{2} 4A_1^\gamma \frac{\partial A_1^\gamma}{\partial V_\alpha} + 5A_2^\gamma \frac{\partial A_2^\gamma}{\partial V_\alpha} + \ldots. \tag{A 6}$$

Substituting for A_n^γ from (A 2)–(A 5) yields

$$-\frac{F_{\rm v}^1}{12\pi\mu} = V_1 - 2V_2 R^{-3} + 3V_1 R^{-6} + 11V_1 R^{-8} + O(R^{-9}). \tag{A 7}$$

The viscous force on bubble 2 is obtained by exchanging V_1 and V_2 in (A 7).

The above expressions for the viscous force on the pair of bubbles agree with those quoted by van Wijngaarden & Kapteyn (1990).

Now we illustrate the method of estimating the viscous forces by the second method described in the main text. In this method we first write the viscous potential as

$$\phi^{\rm v} = \sum_{n=1}^{\infty} \sum_{\alpha=1}^{2} B_n^\alpha \frac{(-1)^n}{n!} \left(\frac{\partial}{\partial x_1}\right)^n \frac{1}{|\boldsymbol{x} - \boldsymbol{x}^\alpha|} \tag{A 8}$$

and solve for B_n^α from the condition (cf. (29))

$$B_n^\alpha = \frac{n}{n+1} C_n^\alpha + 2(2n+1) A_n^\alpha, \tag{A 9}$$

where C_n^α is defined via the expansion of $\phi^{\rm v}$ near the surface of the bubble α as

$$\phi^{\rm v} = \sum_{n=1}^{\infty} (B_n^\alpha s^{-n-1} + C_n^\alpha s^n) P_n(\cos\theta), \tag{A 10}$$

with θ and s measured with respect to the centre of the bubble α and the x_1-axis. It is easy to show that

$$C_n^1 = \sum_{p=1}^{\infty} \frac{(n+p)!}{n!p!} (-1)^n R^{-n-p-1} B_p^2, \tag{A 11}$$

$$C_n^2 = \sum_{p=1}^{\infty} \frac{(n+p)!}{n!p!} (-1)^p R^{-n-p-1} B_p^1. \tag{A 12}$$

Now substituting for C_n^1 from (A 11) and for A_n^α from (A 2)–(A 5) into (A 9) yields values of B_n^1. In particular,

$$B_1^1 = -3V_1 + 6V_2 R^{-3} - 9V_1 R^{-6} - 33V_1 R^{-8} + O(R^{-9}). \tag{A 13}$$

The substitution in $F_{\rm v}^1 = 4\pi\mu B_1^1$ yields the same expression for the force on the bubble as that obtained by the dissipation method (cf. (A 7)). Thus, we see that the two methods yield identical results to $O(R^{-8})$ for the special case of two bubbles aligned in

the direction of their motion. A comparison of the numerical results for the viscous drag obtained by the two methods for N bubbles randomly placed within a unit cell also showed virtually no difference, and hence, we conclude that the two methods are equivalent.

Appendix B. Invariants for potential flow interactions

In the absence of viscous and gravitational forces, certain quantities remain invariant in dynamic simulations. Checking for their invariance provides a good test of the numerical simulations, and therefore we discuss these properties here. The simulations can be carried out for either constant U or constant G. We first consider the former. For this situation, the total momentum and the kinetic energy of the liquid do not remain invariant. Instead the sums of impulses and e^α remain invariant, with e^α defined by

$$e^\alpha = \tfrac{1}{2}[I^\alpha + \rho\sigma^\alpha U]\cdot[v^\alpha - U], \tag{B 1}$$

which reduces to (45) for the special case of $U = 0$, U being the mixture velocity. Denoting the time rate of change of the impulse associated with the bubble α under potential interactions by $\dot{I}^\alpha_{\mathrm{p}}$, we have

$$\dot{I}^\alpha_{i_{\mathrm{p}}} = F^\alpha_{i_{\mathrm{p}}} = \rho \int_{S^\alpha} (\tfrac{1}{2}u_j u_j - u_j v^\alpha_j)\, n_i \,\mathrm{d}A. \tag{B 2}$$

Since $u_j n_j = v^\alpha_j n_j$ on the surface of the bubble, the integral on the right-hand side of (B 2) can also be written as

$$\int_{S^\alpha} (\tfrac{1}{2}u_j u_j n_i - u_i u_j n_j)\,\mathrm{d}A + v^\alpha_j \int_{S^\alpha} (u_i n_j - u_j n_i)\,\mathrm{d}A. \tag{B 3}$$

When $\boldsymbol{u}$ is derived from a gradient of a potential function, the second integral on the spherical surface can be shown to vanish identically, and hence we have

$$\sum_{\alpha=1}^{N} \dot{I}^\alpha_{i_{\mathrm{p}}} = \rho \sum_{\alpha=1}^{N} \int_{S^\alpha} T_{ij} n_j \,\mathrm{d}A, \quad \text{with} \quad T_{ij} = \tfrac{1}{2}u_k u_k \delta_{ij} - u_i u_j. \tag{B 4}$$

Furthermore, it is easy to show that the divergence of T_{ij} vanishes in the liquid when the velocity field is potential. An application of the divergence theorem therefore reduces the sum in (B 4) to an integral of $T_{ij} n_j$ on the surface of the unit cell, and the latter in turn vanishes owing to the periodicity of the velocity field. Consequently, we find that

$$\sum_{\alpha=1}^{N} \dot{I}^\alpha_{i_{\mathrm{p}}} = 0. \tag{B 5}$$

Thus, the sum of impulses remains invariant in the absence of gravitational and viscous forces.

It may be noted here that while the sum of impulses is invariant, the momentum of the liquid does not remain constant for inviscid interactions. The momentum of the liquid within the unit cell can be calculated using the divergence theorem to be

$$\rho \int_{\tau_{\mathrm{f}}} \boldsymbol{u}\,\mathrm{d}V = \sum_{\alpha=1}^{N} I^\alpha_{\mathrm{p}} + \rho \int_{\partial\tau} \phi \boldsymbol{n}\,\mathrm{d}A = \sum_{\alpha=1}^{N} I^\alpha_{\mathrm{p}} + \rho\tau \boldsymbol{G}, \tag{B 6}$$

where τ_{f} is the volume occupied by the liquid and τ is the total volume of the unit cell.

Now $\boldsymbol{G}$ is related to $\boldsymbol{U}$ and $\boldsymbol{D}_1$ via (8) and, for a constant-$\boldsymbol{U}$ simulation, $\boldsymbol{G}$ changes with the sum of the dipoles $\boldsymbol{D}_1$ associated with each bubble. Note that the overall pressure gradient is directly related to $\dot{\boldsymbol{G}}$, and so the pressure gradient across the dispersion is continuously changing during the simulation so as to keep the average velocity of the mixture the same at all times. Corresponding to these pressure changes are changes in the momentum of the liquid, and hence the total momentum of the liquid is not conserved when $\boldsymbol{U}$ is kept constant.

The kinetic energy of the dispersion within one unit cell and be evaluated from

$$K = \tfrac{1}{2}\rho \int_{\tau_f} \frac{\partial \phi}{\partial x_i}\frac{\partial \phi}{\partial x_i}\,\mathrm{d}V = \tfrac{1}{2}\rho \int_{\tau_f} \frac{\partial}{\partial x_i}\left(\phi \frac{\partial \phi}{\partial x_i}\right)\mathrm{d}V. \tag{B 7}$$

Applying the divergence theorem to evaluate the last integral, and simplifying, we finally obtain

$$K = \tfrac{1}{2}\rho G_j U_j \tau + \sum_{\alpha=1}^{N} e^{\alpha} + \tfrac{1}{2}U_i \sum_{\alpha=1}^{N} [(U_i - v_i^{\alpha})\rho\sigma^{\alpha} + I_i^{\alpha}]. \tag{B 8}$$

Since U_i and the sum of impulses is constant during the simulation, we obtain

$$\dot{K} = \rho U_j \dot{G}_j \tau + \sum_{\alpha=1}^{N} \dot{e}^{\alpha}, \tag{B 9}$$

where we have made use of (8). Now an alternative expression for the time rate of change of the total kinetic energy can be obtained by multiplying the Euler equation for the momentum conservation by u_i and integrating the result over the volume of the fluid within a unit cell. Upon using the fact that the force on all the bubbles is zero and that the pressure integral on the boundary of the unit cell is related only to the linearly varying part of ϕ, i.e. to $G_i x_i$, we obtain

$$\dot{K} = \rho U_j \dot{G}_j \tau. \tag{B 10}$$

The above relation simply states that the rate of change of kinetic energy of the liquid equals the work done by the average pressure gradient on the average velocity of the mixture times the density of the liquid. Comparing (B 9) with (B 10), we see that the sum of e^{α} must remain invariant under an inviscid flow interaction.

The above discussion applies to simulations in which the average velocity of the mixture is held constant. If, instead, we require that $\boldsymbol{G}$ is held constant, then it is easy to show that the average velocity of the liquid will remain constant. Also, since the pressure gradient across the unit cell is related to $\dot{\boldsymbol{G}}$, we see that the inviscid pressure drop across the unit cell vanishes. It is easy to show that under this condition, both the sum of impulses and the total momentum remain invariant. The sum of e^{α} as defined by (B 1), on the other hand, does not remain invariant. Instead, the total kinetic energy and the sum of e^{α}, with $e^{\alpha} = \frac{1}{2}(\boldsymbol{I}^{\alpha}\cdot\boldsymbol{v}^{\alpha})$, remain invariant.

REFERENCES

Batchelor, G. K. 1967 *An Introduction to Fluid Dynamics*. Cambridge University Press.

Biesheuvel, A. & Wijngaarden, L. van 1982 The motion of pairs of gas bubbles in a perfect liquid. *J. Engng Maths* **16**, 349.

Davis, R. H., Schonberg, J. A. & Rallison, J. M. 1989 The lubrication force between two viscous drops. *Phys. Fluids* A **1**, 77.

Hasimoto, H. 1959 On the periodic fundamental solutions of the Stokes equations and their application to viscous flow past a cubic array of spheres. *J. Fluid Mech.* **5**, 317.

KANG, I. S. & LEAL, L. G. 1988 The drag coefficient for a spherical bubble in a uniform streming flow. *Phys. Fluids* **31**, 233.

KOK, J. B. W. 1989 Dynamics of gas bubbles moving through liquid. Doctoral thesis, University of Twenty, Enschede, The Netherlands.

LEVICH, V. G. 1962 *Physicochemical Hydrodynamics*. Prentice-Hall.

MOORE, D. W. 1963 The boundary layer on a special gas bubble. *J. Fluid Mech.* **16**, 161.

PROSPERETTI, A. 1977 On the stability of spherically symmetric flows. *Atti della Accademia Nazionale dei Lincei, Rendiconti della Classe di Scienze fisiche, mathematiche e naturali*, vol. 62, p. 196.

SANGANI, A. S. 1991 A pairwise interaction theory for determining the linear acoustic properties of dilute bubbly liquids. *J. Fluid Mech.* **232**, 221.

SANGANI, A. S. & DIDWANIA, A. K. 1993 Dispersed-phase stress tensor in flows of bubbly liquids at large Reynolds numbers. *J. Fluid Mech.* **248**, 27.

SANGANI, A. S. & YAO, C. 1988 Bulk thermal conductivity of composites with spherical inclusions. *J. Appl. Phys.* **63**, 1334.

SANGANI, A. S., ZHANG, D. Z. & PROSPERETTI, A. 1991 The added mass, Basset, and viscous drag coefficients in non-dilute bubbly liquids undergoing small-amplitude oscillatory motion. *Phys. Fluids* A **3**, 2955.

TAM, P. D. 1981 The unsteady drag on a spherical bubble at large Reynolds numbers. *Appl. Sci. Res.* **38**, 245.

WIJNGAARDEN, L. VAN & KAPTEYN, C. 1990 Concentration waves in dilute bubble/liquid mixtures. *J. Fluid Mech.* **212**, 111.